frontiers | Frontiers in Marine Science

TYPE Original Research
PUBLISHED 14 May 2025
DOI 10.3389/fmars.2025.1551655

Check for updates

OPEN ACCESS

EDITED BY
Clifton Buck,
University of Georgia - Skidaway Institute of Oceanography, United States

REVIEWED BY
Debbrota Mallick,
University of Georgia, United States
Jordon Scott Beckler,
Florida Atlantic University, United States

*CORRESPONDENCE
Francisco Delgadillo-Hinojosa
fdelgadillo@uabc.edu.mx

RECEIVED 26 December 2024
ACCEPTED 18 April 2025
PUBLISHED 14 May 2025

CITATION
Delgadillo-Hinojosa F, Félix-Bermúdez A, Torres-Delgado EV, Huerta-Diaz MA, Lares ML, Tovar-Sánchez A, Quijano-del-Olmo SL and Reyes-Bravo MM (2025) Dissolved copper enrichment in the Gulf of Mexico is driven by freshwater inputs, sedimentary fluxes, and cross-shelf exchange induced by Loop Current eddies. *Front. Mar. Sci.* 12:1551655. doi: 10.3389/fmars.2025.1551655



# Dissolved copper enrichment in the Gulf of Mexico is driven by freshwater inputs, sedimentary fluxes, and cross-shelf exchange induced by Loop Current eddies

Francisco Delgadillo-Hinojosa[1*], Armando Félix-Bermúdez[1], Eunise Vanessa Torres-Delgado[1], Miguel Angel Huerta-Diaz[1], Maria Lucila Lares[2], Antonio Tovar-Sánchez[3], Sandra Laura Quijano-del-Olmo[1] and Mauricio Moises Reyes-Bravo[1]

[1]Instituto de Investigaciones Oceanológicas, Universidad Autónoma de Baja California, Ensenada, Mexico, [2]Departamento de Oceanografía Biológica, División de Oceanología, Centro de Investigación Científica y de Educación Superior de Ensenada, Ensenada, Mexico, [3]Departamento de Ecología y Gestión Costera, Instituto de Ciencias Marinas de Andalucía ICMAN-CSIC, Cadiz, Spain

In the ocean, copper functions as an essential micronutrient for primary producers but becomes toxic if its concentration exceeds their cellular requirements. The distribution of copper is strongly controlled by external inputs and physical dynamics, especially in marginal seas with benthic, fluvial, or aeolian sources. We present the spatial distribution of dissolved copper (dCu) in a quasi-zonal transect (25° N) spanning the Gulf of Mexico (GoM) from the Loop Current in the east to the continental slope in the west. The dCu profiles off the continental slope were recorded within a decaying anticyclonic Loop Current eddy (LCE) named Nautilus. In contrast, in the central GoM, dCu profiles were measured on the outside of LCE Olympus, which had recently detached from the Loop Current. The vertical distribution of dCu in the Loop Current was similar to that of the Atlantic Ocean, reflecting the origin of the water entering the GoM. High dCu concentrations in the surface waters of the central GoM were associated with dCu-rich freshwater inputs from the Mississippi River that were transported offshore (>400 km) by LCE Olympus. However, we identified a clear gradient of dCu in surface waters, with the dCu concentration increasing towards the region of LCE Nautilus in the western GoM. The vertical profiles of dCu in the LCE Nautilus also exhibited the highest dCu concentrations and were significantly greater than those of the adjacent Atlantic Ocean. This conspicuous enrichment of dCu was attributed to enhanced off-shelf transport by the decaying LCE Nautilus, in addition to benthic inputs from the continental shelf and slope, with atmospheric fluxes at the surface and the remineralization of organic matter in the water column playing minor roles. Our findings demonstrate that the interaction of mesoscale anticyclonic eddies with the continental margin acts as a mechanism for water exchange between the coastal zone and the deep-water region that is capable of shaping the spatial distribution of dCu in the GoM.

KEYWORDS

**dissolved copper, freshwater inputs, benthic fluxes, aeolian deposition, Loop Current eddies, Gulf of Mexico**

## 1 Introduction

The biogeochemical behavior of copper (Cu) in the marine environment is complicated due to the contrasting roles it plays in phytoplankton physiology, in some cases acting as an essential micronutrient and in other cases acting as a toxic element (Mann et al., 2002; Peers et al., 2005; Peers and Price, 2006; Wu and Lorenzen, 1984). As a micronutrient, Cu acts as a cofactor for several enzymes responsible for electron transport during photosynthesis and respiration, as well as those involved in transmembrane iron transport (La Fontaine et al., 2002; Maldonado et al., 2006; Twining and Baines, 2013). However, if the Cu concentration in seawater exceeds the cellular requirements of phytoplankton, it can become toxic to these and other marine microorganisms (Jordi et al., 2012; Paytan et al., 2009; Wang et al., 2017). Copper toxicity has been mainly associated with the free $Cu^{2+}$ ion, which has been shown to inhibit phytoplankton growth (Mann et al., 2002; Sunda and Ferguson, 1983). However, $Cu^{2+}$ can interact with dissolved organic matter and form strong organic complexes, thus lowering its toxicity to phytoplankton (Bruland et al., 2014). This buffering effect restricts the biological uptake of Cu and prevents its depletion in seawater, ultimately influencing the distribution of Cu in the ocean (Arnone et al., 2023; Bruland et al., 2014; Jacquot and Moffett, 2015; Ruacho et al., 2022; Wong et al., 2021).

The Gulf of Mexico (GoM; Figure 1) is a complex marginal sea in which physical mesoscale dynamics, biogeochemical processes, and external inputs (fluvial, atmospheric, and sedimentary) interact and collectively modulate the distributions of essential trace elements, including Cu. In particular, the large anticyclonic mesoscale eddies that are shed from the Loop Current (LCEs) are key oceanographic features that must be considered to understand these interactions. These eddies, which are characterized by clockwise rotations, isopycnal sinking at their cores, and westward trajectories (Vukovich, 2007), are able to trap water masses and transport them over large distances across the gulf. On their westward journey, LCEs can interact with the coastal zone after detaching from the Loop Current. Some LCEs move northward, putting them on course to interact with the coastal zone of the northern GoM (Brokaw et al., 2019; Otis et al., 2019), which is the region with the greatest freshwater inflow into the system (Gierach et al., 2013; Hu et al., 2005; Vance et al., 2008). In the same way, at the end of their travel to the west, others LCEs end up colliding with the slope and narrow continental shelf of the western GoM (Guerrero et al., 2020; Vidal et al., 1992, Vidal et al., 1994; Zavala-Hidalgo et al., 2003). Thus, given their rotational motion and trajectories, the interaction of LCEs with the continental margin is likely an important physical mechanism that exchanges water and biogeochemical constituents between the coastal zone and the interior of the GoM. Currently, little is known regarding the magnitude of water exchange between LCEs and the coastal zone, as well as the potential impacts of this exchange on the spatial distribution of dissolved trace metals in the deep region of the GoM.

It is well known that Cu, and other trace metals, enter the GoM via several routes including a) fluvial inputs from the Atchafalaya–Mississippi River system, located in the northern gulf (Boyle et al., 1984; Buck et al., 2015; Joung and Shiller, 2016; Mallick et al., 2022; Wen et al., 2011), b) the atmospheric deposition of particles from the Sahara Desert that cross the Atlantic Ocean (Ebling and Landing, 2017; Lenes et al., 2001; Scott et al., 2022) and those from the North American landmass surrounding the gulf (Bozlaker et al., 2013, Bozlaker et al., 2019; Hayes et al., 2022), and c) the benthic fluxes from the continental shelf and slope of the gulf (e.g., Boyle et al., 1984). The semi-enclosed nature of the GoM and the strong interaction of its water masses with the continental margin suggest that shelf and slope sediments could be a prominent source of metals, potentially exceeding the contribution of dust deposition (Hayes et al., 2022). The extensive and steep continental margin in the gulf facilitates the lateral transport of lithogenic particles, such as those found in nepheloid layers (Diercks et al., 2018), as well as the release of dissolved metals through benthic fluxes (Boyle et al., 1984; Lenstra et al., 2022). These metal-rich waters (potentially Cu-enriched) might be transported by LCEs into the deep-water region of the GoM, as has been reported for the transport of biogenic particles (Daudén-Bengoa et al., 2024) and freshwater plumes (e.g., Brokaw et al., 2019). Altogether, the interactions between these external sources of Cu and LCEs could increase the variability and, consequently, complicate our understanding of the spatial distribution of dissolved Cu (dCu) in the deep-water region of the GoM.

This work examined the combined impact of LCEs and external fluvial, atmospheric, and benthic inputs on the horizontal and

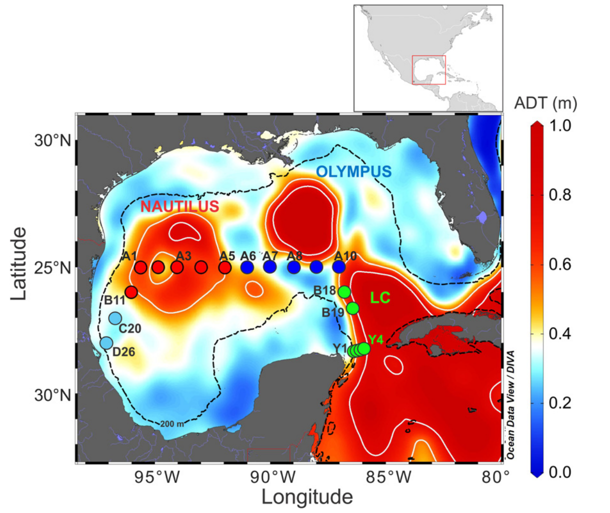


FIGURE 1
Map of the Gulf of Mexico (GoM) showing the sampling stations along the transect during the first leg of the XIXIMI-4 cruise. Sampling started at station D26 near the eastern coast of Mexico on 27 August 2015 and ended at station Y1 in the Yucatan Channel on 3 September 2015. Spatial distribution of satellite-derived absolute dynamic topography (ADT; color scale) on 31 August 2015. The Loop Current Eddies (LCEs) Nautilus and Olympus (Woods Hole Group; https://www.horizonmarine.com/loop-current-eddies) were geographically located by tracing the most external and internal ADT isolines of 0.55 m and 0.8 m, respectively. The 200 m depth contour at the shelf break is also shown. The stations were colored according to the oceanographic provinces identified during the campaign: Loop Current (LC; green circles), south of LCE Olympus (blue circles along 25° N), and LCE Nautilus (red circles). The figure was generated with Ocean Data View (Schlitzer, 2024).

vertical distribution of dCu in the upper 1000 m of the water column of the deep-water region of the GoM. We were particularly interested in examining how the spatial variability of dCu is influenced as detached mesoscale eddies transport water from the Loop Current and, during their westward journey, interact with the continental margin of the Gulf. To this end, a quasi-zonal transect (1,700 km) was sampled that extended from the Loop Current in the east to the continental slope of Mexico in the west. The transect included sampling stations along the southern edge of a recently detached LCE (Olympus) in the central gulf and stations that traversed an LCE in decay (Nautilus) in the west. In general, a clear east-west gradient of dCu was identified, with the highest surface dCu concentrations recorded in the areas influenced by the LCEs, revealing the influence of fluvial sources in the northern GoM and the continental margin in the western GoM. The highest dCu concentrations in all vertical profiles were identified in the region of LCE Nautilus, which were also significantly higher than those in the Atlantic Ocean. This conspicuous dCu enrichment was attributed to the impact of off-shelf transport from the decaying LCE Nautilus and sedimentary inputs from the continental shelf and slope of the western gulf. Our results improve our understanding of the impacts of mesoscale dynamics and external inputs on the spatial distributions of essential trace metals along LCE pathways and provide valuable insights into the biogeochemical cycling of Cu in the GoM.

# 2 Materials and methods

## 2.1 Study area

The GoM (18–30° N; 82–98° W) is a subtropical marginal sea that is connected to the Caribbean Sea and Atlantic Ocean. This semi-enclosed basin spans ~1.6 × $10^6$ $km^2$ (Muller-Karger et al., 2015) and reaches depths >3500 m in the Sigsbee Abyssal Plane (Pérez-Brunius et al., 2018). The GoM is bordered to the north by the United States, to the east by Cuba, and to the west and south by Mexico (Figure 1). The waters that enter the GoM, which come from the North Atlantic western boundary current system (Candela et al., 2019), flow through the Caribbean Sea before being transported into the gulf by the intense Loop Current (Candela et al., 2002). Water flows out of the GoM through the Florida Straits and becomes part of the Gulf Stream (Muller-Karger et al., 2015; Schmitz and McCartney, 1993).

### 2.1.1 The Loop Current and anticyclonic mesoscale eddies

The Loop Current is responsible for the predominant mesoscale pattern in the GoM. This warm water current flows northward into the GoM through the Yucatan Channel and makes an anticyclonic turn before exiting the gulf through the Florida Straits (Candela et al., 2019), shedding large anticyclonic LCEs as it moves through the gulf. These LCEs, which can reach diameters of 200–400 km, detach irregularly at variable intervals of 4–18 month (Leben, 2005) and are frequently observed surrounded by much smaller cyclonic and anticyclonic mesoscale eddies (Sturges and Leben, 2000). After detaching, LCEs move westward across the gulf (Vukovich, 2007) while rotating clockwise at speeds of 2–5 km·$d^{-1}$ (Elliott, 1982; Vukovich and Crissman, 1986). Eventually, LCEs dissipate when they collide against the slope and the continental shelf on the western GoM (Hamilton et al., 1999; Vidal et al., 1992, Vidal et al., 1994; Zavala-Hidalgo et al., 2003), a region that has been referred to as an eddy graveyard by some authors.

Given that LCEs transport warm waters (Caribbean Surface Water [CSW]) and saline waters (North Atlantic Subtropical Underwater [NASUW]) coming from the Caribbean Sea to the western region of the GoM, they play important roles in modulating the heat and salt balances of the gulf (Meunier et al., 2018). In fact, LCEs regulate the distribution of water masses in the central and western regions of the gulf (Portela et al., 2018) because of their ability to trap and transport those water masses–and their chemical and biological characteristics–away from their formation sites at the Loop Current (Félix-Bermúdez et al., 2023; Lee-Sanchez et al, 2022; Linacre et al., 2019; Meunier et al., 2021), which may have important biogeochemical implications for the gulf.

### 2.1.2 Freshwater inputs to the Gulf of Mexico

The GoM receives freshwater inputs from several major rivers based on their discharge volumes, with the Mississippi River contributing the largest flow (mean = 13,500 $m^3$·$s^{-1}$) and accounting for ~41% of the input of inland water into the GoM (Gierach et al., 2013; Hu et al., 2005; Osburn et al., 2019; Vance et al., 2008). River discharge is typically highest in late winter and spring due to the runoff generated by continental melting during these seasons and clearly decreases towards the summer (Gierach et al, 2013). The large watershed of the Mississippi River drains multiple regions of the United States that include agricultural, industrial, and urban areas, and the discharge from this river contributes substantial amounts of organic matter, nutrients, and trace metals to the coastal zone of the northern GoM (Joung et al., 2019). The arrival of freshwater from the Mississippi River to this region of the gulf creates low-salinity plumes (<36 g·kg$^{-1}$) that can extend over large sections of the continental shelf (Hu et al., 2005; Morey et al., 2003) and reach the deep zone of the gulf through interactions with winds and mesoscale eddies (Otis et al., 2019). These freshwater plumes are associated with high concentrations of dissolved substances, including dCu (20–36 nmol·kg$^{-1}$; e.g., Shiller and Boyle, 1991; Gaillardet et al., 2014), which may especially affect the local and regional biogeochemistry of Cu in the GoM.

#### 2.1.3 Atmospheric circulation and particle supply to the Gulf of Mexico

The winds in the GoM stand out for their high spatiotemporal variability, their notable influence on water circulation (Zavala-Hidalgo et al., 2014), and their influence on the supply and transport of particulate matter in the surface waters of the gulf (Hayes et al., 2022). During summer, wind circulation is primarily influenced by the North Atlantic High (commonly known as the Bermuda High). This high-pressure system, which is located over the eastern GoM, causes the trade winds to prevail predominantly from the southeast during summer, given the counterclockwise flow around the North Atlantic High (Prospero, 1999; Metcalfe et al., 2015). These winds bring warm and humid air masses from the Caribbean Sea and Atlantic Ocean to the GoM and tend to be relatively constant (Metcalfe et al., 2015). However, the winds can be disrupted by tropical cyclones, which frequently occur from June to November during the Atlantic hurricane season (Patricola et al., 2024).

Winds carry loads of particulate matter to the GoM. Indeed, minerals in the form of fine dust containing silicate minerals, iron oxides (Bozlaker et al., 2019; Prospero, 1999; Prospero et al., 1981), and associated trace metals (Hayes et al., 2022; Scott et al., 2022), are transported across the Atlantic Ocean from the Sahara Desert. During the summer months, atmospheric circulation increases the delivery of this dust to the western Atlantic Ocean and GoM (Tong et al., 2023). Additionally, aerosol emissions from the industrial and agricultural activities of continental North America (Ren et al., 2014; Bozlaker et al., 2019) are important sources of particulate matter to the atmosphere. This particulate matter subsequently reaches the GoM through wet and dry deposition processes. Once deposited on the sea surface, mineral dust and anthropogenic aerosols can solubilize, increasing the concentrations of elements, such as Fe (Lenes et al., 2001, Lenes et al., 2012) or Cu (Ebling and Landing, 2017; Mellett and Buck, 2020), especially during periods of high dust flux or industrial activity.

## 2.2 Material cleaning

The collection and handling of seawater samples, their processing in the laboratory, and dCu quantification required the use of trace metal clean procedures (Bruland et al., 1979; Delgadillo-Hinojosa et al., 2001; Delgadillo-Hinojosa et al., 2006; Tovar-Sanchez, 2012), similar to GEOTRACES cleaning protocols (e.g., Cutter et al., 2017). The plastic labware was washed with 3% Micro-90 soap, rinsed with distilled water, and kept immersed in 3% Micro-90 soap solution for one week. Then, the plastic material underwent a two-stage acid bath that consisted of a four-week immersion in 9% HCl (reagent grade; Mallinckrodt Baker, Inc. [J.T. Baker®], Phillipsburg, USA) followed by a one-week immersion in 5% $HNO_3$ Ultrex (JT Baker®). Between each acid solution change, the plastic material was rinsed using copious amounts of deionized water (DIW; >18.2 MΩ-cm). Final drying was conducted in a laminar flow hood (class 100; Envirco, Sanford, USA) (Segovia-Zavala et al., 1998; Segovia-Zavala et al., 2010). The Niskin-X bottles (General Oceanics Inc., Miami, USA) that were used to collect water during hydrographic casts were subjected to the rigorous cleaning process described by Félix-Bermúdez et al. (2023). The low-density polyethylene bottles that were used to store water samples for dCu analysis were filled with a diluted solution of $HNO_3$ Ultrex (0.01 M; JT Baker®), which was discarded prior to seawater collection during the hydrographic cruise. Finally, all bottles were stored in double plastic bags and transported to the ship in sealed plastic buckets until they were used during the campaign.

## 2.3 Experimental design and hydrographic sampling

The first leg of the XIXIMI-4 cruise took place from 27 August 2015 to 3 September 2015 in the deep-water region of the GoM (>1000 m) aboard the RV Justo Sierra (hereinafter referred to as XIXIMI-4). In all, 19 hydrographic stations were sampled along a transect that extended from the Yucatan Channel in the east to the western coast of the GoM (Figure 1). Vertical temperature, conductivity, and pressure profiles were recorded at each station with a SeaBird SBE 9 Plus CTD (SeaBird Scientific, Bellevue, USA) equipped with dissolved oxygen ($dO_2$; SBE 43), chlorophyll fluorescence (chlorophyll fluorometer, Seapoint Sensors Inc., Exeter, USA), and chromophoric dissolved organic matter (cdom; ECO FLRTD fluorometer, Wet Labs, Corvallis, USA) sensors. Water samples were collected at each station for trace metal analysis using acid-cleaned, 20-L Niskin-X bottles (General Oceanics Inc.) mounted on an epoxy-coated SBE 32 rosette (SeaBird Scientific). Water was collected at 6 different depths: 10 m, 30–100 m (fluorescence maximum), 150 m, 400–500 m (oxygen minimum), 600 m, and 1000 m. Once on deck, the Niskin-X bottles were fitted with Acro®50 vent filters (Cytiva, Marlborough, USA) with a 0.2-mm PTFE membrane to prevent contamination from the atmosphere on the ship. Each seawater sample was transferred by an acid-cleaned silicone hose and peristaltic pump into a clean room equipped with a laminar flow hood and filtered through acid-cleaned AcroPack™ 200 cartridge with a 0.2-µm Supor® membrane (Cytiva). Before the final sample was collected, the acid-cleaned low-density polyethylene bottles were rinsed three times with the filtered seawater. Then, the final sample (1000 mL) was collected and acidified to pH < 2 by adding 1 mL Ultrex $HNO_3$ (JT Baker®). Finally, the bottles were stored in double Ziploc® plastic bags and placed in airtight polyethylene buckets for transport to the onshore laboratory. Water samples were stored for about 6 months before chemical analysis.

## 2.4 Dissolved Cu analysis

The samples intended for dCu analysis were processed in an ultra-clean laboratory inside a laminar flow hood (class 100, NuAire, Plymouth, USA) following a metal preconcentration procedure by organic extraction (Bruland et al., 1979; Félix-Bermúdez et al., 2020, Félix-Bermúdez et al., 2023; Moffett and Zika, 1988; Segovia-Zavala et al., 2010; Tovar-Sanchez, 2012). Briefly, a 250-mL aliquot of seawater was poured into a 500-mL Teflon separatory funnel, and the pH was adjusted to 4.5 with ammonium acetate ($CH_3COONH_4$). Subsequently, 1 mL of an APDC (1% ammonium pyrrolidine dithiocarbamate)/DDDC (1% diethylammonium diethyldithiocarbamate) solution was added as a complexing agent, which had been previously cleaned with chloroform ($CHCl_3$; HPLC grade) subjected to a wash with DIW. Then, 8 mL of $CHCl_3$ was added, manually stirred for 2 min, and left to stand for 5 min. The $CHCl_3$ was recovered in a 125-mL separatory funnel. This procedure was repeated with 6 mL of $CHCl_3$, which was recovered in addition to the 8 mL of $CHCl_3$ recovered in the previous step. A total of 100 µL of Ultrex II grade $HNO_3$ (J.T. Baker®) was added to the 14 mL of $CHCl_3$ to release Cu from the organic complex. Then, 3 mL of DIW were added to increase the volume of the acid phase; the mixture was manually shaken for 1 min and left to stand for 5 min. Finally, the acid extract was recovered in an acid-cleaned, 8-mL polyethylene bottle. The quantification of dCu in the extracts was performed by inductively coupled plasma-mass spectrometry (ICP-MS) with an ICAP Q mass spectrometer (Thermo Fisher Scientific, Waltham, USA) using external standards and rhodium as the internal standard (Félix-Bermúdez et al., 2023; Tovar-Sanchez, 2012).

## 2.5 Quality control

To assess the accuracy and precision of our analytical procedure, we analyzed certified seawater standards (NASS-7; North Atlantic Surface Seawater from the National Research Council of Canada) and procedural blanks (DIW >18.2 MΩ-cm). The dCu concentration measured in the NASS-7 reference material (3.07 ± 0.29 nmol·kg $^{-1}$) was similar to the certified value (3.01 ± 0.14 nmol·kg$^{-1}$), with a recovery percentage of 98.1 ± 4.7%. Precision, expressed as the coefficient of variation from four replicate analyses of NASS-7, ranged between 2% and 5%. The detection limit, defined as three times the standard deviation of the procedural blank, was 0.026 nmol·kg$^{-1}$, which was <4% of the lowest dCu value reported in this work. Dissolved Cu levels in procedural blanks were consistently below the detection limit of the method.

## 2.6 Hydrographic data processing

The temperature and salinity data obtained from the CTD were processed to 1-m resolution and converted to conservative temperature (TC) and absolute salinity ($S_A$) using the TEOS-10 equations (McDougall and Barker, 2011). The dissolved oxygen sensor readings were calibrated with measurements obtained with the micro-Winkler method (accuracy: 0.1%; precision: ~1.3 µmol·kg$^{-1}$; Valencia-Gasti et al., 2022). A dCu vs $S_A$ analysis was also performed to evaluate the behavior of surface dCu along the salinity gradient between the marine endmember of the GoM (seawater from the Loop Current) and the riverine endmember (freshwater from the Mississippi River) in the northern GoM.

## 2.7 Satellite-derived absolute dynamic topography and sea surface salinity

Daily absolute dynamic topography (ADT; m) and the geostrophic velocity components ($u$ and $v$; m s$^{-1}$) were obtained from sea level gridded data from satellite observations for the global ocean (https://cds.climate.copernicus.eu/datasets/satellite-sea-level-global?tab=overview). The spatial resolution of the images was 0.25° × 0.25°, and they were downloaded for the period of 27 August 2015 to 3 September 2015. In addition, soil moisture active passive (SMAP) level-3 (L3) sea surface salinity (SSS) data for the same dates were retrieved from the Physical Oceanography Distributed Active Archive Center of NASA (https://search.earthdata.nasa.gov/). This product has global coverage and is gridded at an 8-day time scale and spatial resolution of 0.25° × 0.25° (Brokaw et al., 2019; da Silva and Castelao, 2018; Vazquez-Cuervo et al., 2018). Satellite-derived ADT and SSS data were used to define the distribution and spatial extent of the mesoscale eddies during XIXIMI-4.

## 2.8 Meteorological data, air mass back-trajectories, and aerosol optical depth

To identify the potential origin of atmospheric particles that arrived in the study area during the cruise, air mass back-trajectories (AMBTs) were computed using the Hybrid Single Particle Lagrangian Integrated Trajectory (HYSPLIT) model (Draxler and Hess, 1998; Stein et al., 2015). The meteorological data fields used for the model were downloaded from the National

Climatic Data Centre's (NCDC) website. We used the Global Data Assimilation System (GDAS) meteorological data (gdas0p5), which had a horizontal resolution of 0.5° × 0.5°. Thus, daily AMBTs were obtained considering a 5-day travel period per trajectory and arrival heights of 100 m and 500 m above sea level at the sampling stations. The arrival heights were chosen to represent the trajectories within the marine boundary layer (Ebling and Landing, 2017), i.e., that part of the atmosphere that has direct contact and is directly influenced by the ocean. In addition, daily aerosol optical depth (AOD) data were retrieved from the Moderate Resolution Imaging Spectroradiometer (MODIS) L3 AOD products of the Aqua satellite (https://giovanni.gsfc.nasa.gov/giovanni/). AOD is a dimensionless number that measures light extinction along a vertical path through the atmosphere over the sampling station due to the presence of aerosols (e.g., Kenlee et al., 2024). The spatial resolution of the gridded dataset (MYD08_D3) was 1° × 1°, and the data spanned the period of 26 August 2015 to 4 September 2015.

## 2.9 Statistical analysis

Statistical analyses of the differences between zones (or depths) for physical (Tc, $S_A$, $\sigma_t$, and ADT), biological (fluorescence), or chemical (dCu, $dO_2$, AOU, and cdom) variables were performed using Student t-tests or Wilcoxon tests, depending on whether the data met the assumptions of normality or homoscedasticity, which were evaluated with the Shapiro-Wilk and Levene tests, respectively. The degree of association between any two variables was quantified using the Pearson correlation coefficient. A linear regression analysis was also performed to evaluate the existence of a longitudinal gradient in the dCu concentration along the transect. The results of each test were considered statistically significant if $p < 0.05$. All statistical analyses were performed using R statistical software (R Core Team, 2024).

# 3 Results

## 3.1 Hydrographic conditions during the summer 2015

The spatial distribution of ADT during XIXIMI-4 allowed us to unambiguously identify the Loop Current entering the gulf in the east, LCE Olympus in the north-central region of the GoM, and LCE Nautilus to the west (Figure 1). LCE Olympus, which was located to the north of 25° N, had recently detached from the Loop Current, and measurements of this LCE were only taken in its southern and outer portions. LCE Nautilus, which detached from the Loop Current in May 2015 (Hamilton et al., 2018), had travelled westward across the GoM for four months. At the time of sampling, this eddy was colliding with the slope and the continental shelf off the western coast of the GoM and, consequently, was in decay. In what follows, this categorization will be used to distinguish the oceanographic provinces present during XIXIMI-4 and to describe the impacts of mesoscale dynamics on the spatial distribution of dCu during the summer of 2015.

## 3.2 Water masses present in the transect

Figure 2A presents the $T_C$-$S_A$ for the first 1000 m of the GoM during XIXIMI-4. Six water masses were detected in this upper layer of the water column according to the classification of Portela et al. (2018): Caribbean Sea Water (CSW), Gulf Common Water (GCW), North Atlantic Subtropical Underwater (NASUW), Tropical Atlantic Central Water (TACW), Antarctic Intermediate Water (AAIW), and North Atlantic Deep Water (NADW). Notably, a freshwater plume coming from the north of the gulf was detected at the surface in a section to the south of LCE Olympus (Figures 2B, C), more than 450 km away from the coast. This low-salinity and cdom-enriched plume extended from A7 to A10. The lowest salinity (33.21 $g{\cdot}kg^{-1}$) and highest cdom concentration (2.13 $mg{\cdot}m^{-3}$) were recorded in A8 at 10 m depth.

Below the surface, the cdom isolines, isopycnals and upper and lower boundaries of water masses exhibited vertical displacement, which was a function of mesoscale eddy activity (Figures 2B–D; Table 1; Supplementary Figure S1B). For example, in the LCE Nautilus region, CSW ($\sigma_t$ ~ 24 $kg{\cdot}m^{-3}$) was found between 53 m and 103 m, whereas south of LCE Olympus, the upper and lower boundaries of this water mass were 25 m and 57 m, respectively. Below CSW, the core of high salinity ($S_A$ > 36.8 $g{\cdot}kg^{-1}$) that characterizes NASUW ($\sigma_t$ ~ 25.5 $kg{\cdot}m^{-3}$) was located in the eastern region of the gulf (Figures 2A, B). The upper boundary of NASUW varied from 102 m in the Loop Current to 54 m south of LCE Olympus. In the west, at approximately the same depths as NASUW, the upper boundary of GCW ($\sigma_t$ ~ 25.5 $kg{\cdot}m^{-3}$) ranged from 104 m at LCE Nautilus to 62 m south of LCE Olympus. Immediately below this water mass, TACW exhibited an oxygen minimum zone (OMZ) and the greatest thickness (~430 m) of all water masses in the upper 1000 m of the water column (Figures 2A, B, D). The upper boundary of TACW ($\sigma_t$ ~ 26.0 $kg{\cdot}m^{-3}$) was shallow south of LCE Olympus (113 m) and deeper (160 m) in the region of LCE Nautilus. The vertical displacement of this isopycnal revealed that the most dramatic deepening of the upper boundary of the OMZ occurred in the area of LCE Nautilus, whereas an elevation of the upper boundary of the OMZ was detected south of LCE Olympus (Figure 2D). AAIW ($\sigma_t$ ~ 27.5 $kg{\cdot}m^{-3}$; Table 1), which was identified by the minimum absolute salinity ($S_A$ = 35.05 $g{\cdot}kg^{-1}$; Figure 2A), was located in the last third of the water column from 714 m to 911 m. Finally, in the deepest part of the transect, the low temperatures of NADW dominated below 900 m (Table 1).

## 3.3 Dissolved Cu enrichment in the western GoM

The horizontal distribution of dCu in the top 150 m of the water column exhibited a clear gradient, generally increasing from east to west (Figure 3B). The lowest surface water dCu values were measured in the region of the Loop Current ($\bar{x}$ = 1.07 ± 0.04 $nmol{\cdot}kg^{-1}$), with intermediate levels south of LCE Olympus and the highest levels in the region of LCE Nautilus ($\bar{x}$ = 2.07 ± 0.24 $nmol{\cdot}kg^{-1}$). However, unlike those in the samples collected from the

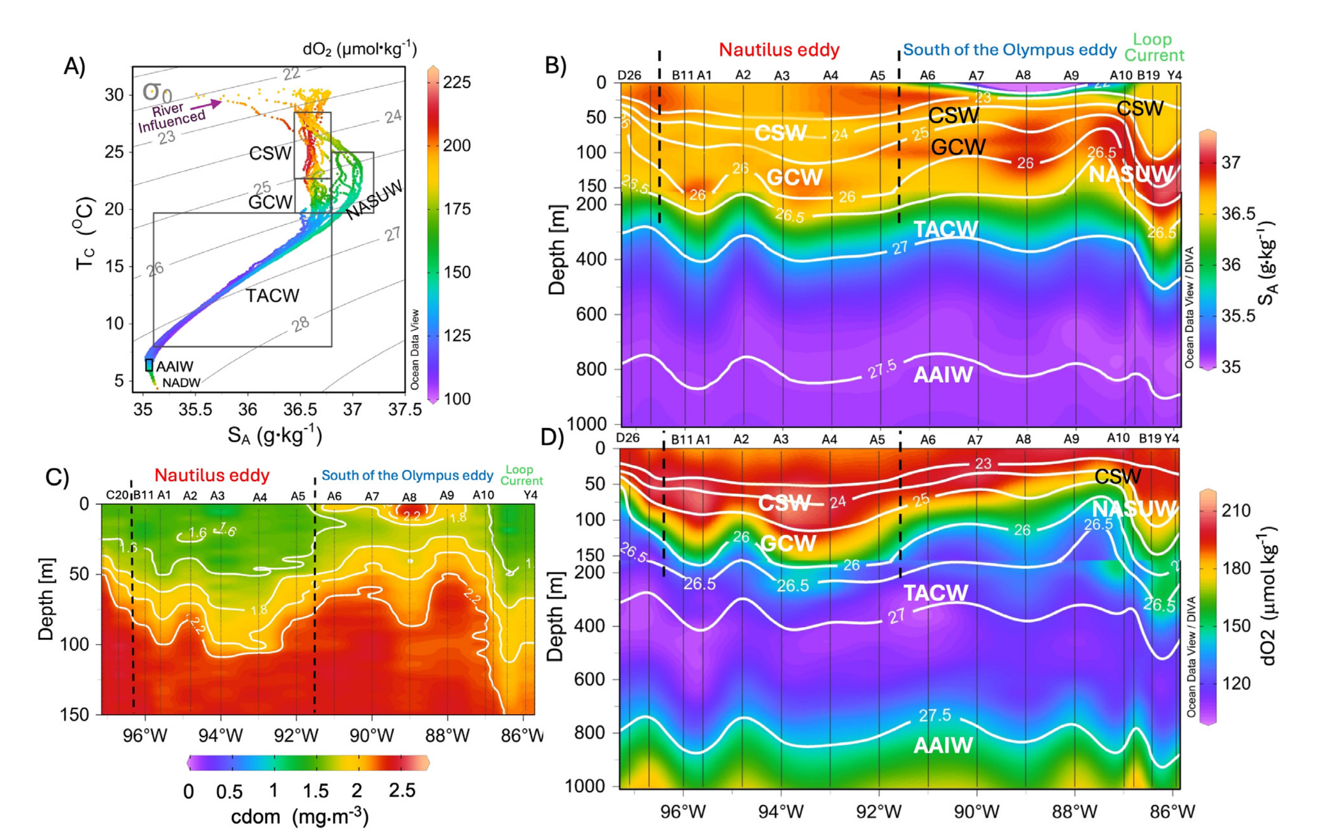


FIGURE 2
**(A)** Conservative temperature–absolute salinity (Tc–$S_A$) diagram, and sectional distribution of **(B)** absolute salinity ($S_A$), **(C)** chromophoric dissolved organic matter (cdom) and **(D)** dissolved oxygen ($dO_2$) during the first leg of the XIXIMI-4 cruise. In panels **(B–D)**, the sampling station positions are shown at the top, and the black vertical dashed lines show the approximate extension of LCE Nautilus. Potential density anomalies ($\sigma_t$) are drawn as white solid lines in panels **(B, D)**. Note that the sectional distribution of cdom is shown for the upper 150 m layer in panel **(C)**. The water masses present in the GoM were identified according to the classification of Portela et al. (2018): Caribbean Sea Water (CSW), Gulf Common Water (GCW), North Atlantic Subtropical Underwater (NASUW), Tropical Atlantic Central Water (TACW), and Antarctic Intermediate Water (AAIW). This figure was generated with Ocean Data View (Schlitzer, 2024).

fluorescence maximum and 150 m, the dCu values at 10 m depth exhibited higher spatial variability (Figures 3A, B). For example, in the eastern portion of the transect, the highest surface concentrations of dCu were recorded at stations A8 (5.30 nmol·kg$^{-1}$) and A10 (3.73 nmol·kg$^{-1}$) south of LCE Olympus, where the lowest salinities were observed (Figures 3A, B, 4A–C). This suggests that the spatial variability of dCu at the surface was associated with the signal of freshwater inputs from the coastal zone. In contrast, in the area of LCE Nautilus, the high dCu levels at the surface in stations B11 (5.49 nmol·kg$^{-1}$) and A1 (2.70 nmol·kg$^{-1}$) were associated with the high salinities recorded in this region of the gulf Figures 3A, B, 4A–C). Thus, in addition to the influence of fluvial inputs, there may be other external sources that supply dCu to the surface waters of the gulf such as sedimentary fluxes or the atmospheric deposition of dust or aerosols.

Between 150 m and 600 m depth, TACW intrusion was observed from the Yucatan Channel, with very low dCu values associated with the OMZ (Figures 3A, 2D; Supplementary Figure S1A). This dCu minimum ($\bar{x}$ = 1.10 ± 0.08 nmol·kg$^{-1}$) in the OMZ was found to extend west to station A3. However, upon arriving to the west of LCE Nautilus, the dCu concentration in this layer (including stations A2, A1, and B11) significantly increased ($\bar{x}$ = 1.82 ± 0.26 nmol·kg$^{-1}$; $t_{student}$, $p < 0.001$) (Figures 3A, C). Thus, dCu enrichment in the western GoM occurred not only at the surface but also in the subsurface layers, likely associated with the interaction of LCE Nautilus and the continental margin of the western GoM. Finally, the dCu concentration at 1000 m depth along the entire transect was somewhat variable and, relative to the dCu minimum in the OMZ, was slightly elevated ($\bar{x}$ = 1.59 ± 0.35 nmol·kg$^{-1}$) (Figures 3A, D-F; Supplementary Figure S1A).

# 4 Discussion

## 4.1 Vertical distribution of dCu in the GoM

The vertical distribution of dCu in the upper 1000 m of the Loop Current, south of LCE Olympus, and in the region of LCE Nautilus, is shown in Figures 3D–F and Table 1. The average dCu profile in the Loop Current was nearly vertically homogeneous (~1.10 nmol·kg$^{-1}$), reflecting the intense physical dynamics characteristic of this zone as evidenced by typical geostrophic

TABLE 1 Average (± standard deviation) of conservative temperature (Tc), absolute salinity ($S_A$), potential density anomaly (σt), apparent oxygen utilization (AOU), dissolved copper (dCu), and the upper and lower depth limits of the water masses recorded during the first leg of the XIXIMI-4 cruise.

| Water mass | Region | Upper–lower depth | $T_C$ | $S_A$ | σt | AOU | dCu |
|---|---|---|---|---|---|---|---|
| | | (m) | (°C) | ($g \cdot kg^{-1}$) | ($kg \cdot m^{-3}$) | ($\mu mol \cdot kg^{-1}$) | ($nmol \cdot kg^{-1}$) |
| CSW | LC | 40–86 | 27.5 (0.7) | 36.61 (0.08) | 23.63 (0.26) | 1.5 (8.1) | 1.12 (0.14) |
| | South-OE | 25–57 | 25.8 (1.7) | 36.60 (0.13) | 24.15 (0.59) | -1.0 (13.2) | 1.49 (0.22) |
| | Nautilus-E | 53–103 | 25.0 (1.6) | 36.60 (0.05) | 24.40 (0.51) | -3.9 (12.9) | 1.97 (0.53) |
| GCW | LC | – | – | – | – | – | – |
| | South-OE | 62–99 | 21.1 (0.8) | 36.67 (0.06) | 25.60 (0.25) | 49.2 (21.9) | 1.61 (0.30) |
| | Nautilus-E | 104–159 | 21.1 (0.8) | 36.66 (0.06) | 25.59 (0.24) | 46.5 (19.2) | 1.75 (0.26) |
| NASUW | LC | 102–162 | 22.1 (1.6) | 36.98 (0.07) | 25.55 (0.43) | 58.1 (13.3) | 0.95 (0.19) |
| | South-OE | 54–119 | 21.7 (1.6) | 36.91 (0.06) | 25.59 (0.46) | 58.3 (14.6) | – |
| | Nautilus-E | – | – | – | – | – | – |
| TACW | LC | 181–565 | 12.8 (3.2) | 35.80 (0.51) | 26.87 (0.27) | 127.2 (30.2) | 0.97 (0.10) |
| | South-OE | 113–567 | 12.3 (3.2) | 35.71 (0.48) | 26.91 (0.29) | 139.1 (23.7) | 1.16 (0.17) |
| | Nautilus-E | 160–601 | 12.3 (3.3) | 35.73 (0.48) | 26.91 (0.32) | 142.9 (27.3) | 1.54 (0.40) |
| AAIW | LC | 778–911 | 5.9 (0.3) | 35.07 (0.01) | 27.49 (0.04) | 151.5 (4.8) | 1.19 (0.02) |
| | South-OE | 714–858 | 5.9 (0.3) | 35.08 (0.01) | 27.49 (0.04) | 156.5 (4.6) | – |
| | Nautilus-E | 744–896 | 6.0 (0.3) | 35.08 (0.00) | 27.49 (0.04) | 156.5 (4.4) | – |
| NADW | LC | 958 | 5.0 (0.2) | 35.10 (0.01) | 27.63 (0.04) | 134.8 (5.2) | 1.36 (0.13) |
| | South-OE | 904 | 5.0 (0.2) | 35.10 (0.01) | 27.62 (0.02) | 139.8 (4.0) | 1.65 (0.42) |
| | Nautilus-E | 941 | 5.1 (0.1) | 35.10 (0.01) | 27.61 (0.02) | 141.2 (3.2) | 1.69 (0.34) |

Statistical parameters were calculated using all data available within the oceanographic zones identified during the campaign: Loop Current (LC), south of the Loop Current Eddy (LCE) Olympus (South-OE), and region of LCE Nautilus (Nautilus-E). Water masses: Caribbean Sea Water (CSW), Gulf Common Water (GCW), North Atlantic Subtropical Underwater (NASUW), Tropical Atlantic Central Water (TACW), Antarctic Intermediate Water (AAIW), and North Atlantic Deep Water (NADW).

velocities of >0.5 $m \cdot s^{-1}$ (Figure 4A, Manta et al., 2023). A comparison with the average dCu profile of the GA03 cruise (purple stars in Figures 3D, F) revealed that the vertical distribution of dCu in the Loop Current showed a slight surface maximum and, below 100 m depth, was similar to that of the North Atlantic (Roshan and Wu, 2015). In contrast, in the stations south of LCE Olympus and in the region of LCE Nautilus, the dCu concentration exhibited a clear surface maximum, decreased in subsurface waters, and reached its lowest values within the OMZ at depths between 300 m and 600 m (Figures 3D, E). Furthermore, in the region influenced by LCE Nautilus, the dCu profiles exhibited high spatial variability and, when compared with those of the Loop Current (this study; Boyle et al., 1984) or North Atlantic (Roshan and Wu, 2015), a notable enrichment of dCu was observed throughout the water column (Figure 3D). In the following sections, we argue that these features of the spatial distribution of dCu are explained by the surface fluvial inputs of Cu as well as benthic fluxes combined with the physical dynamics generated by mesoscale eddies when interacting with the continental shelf and slope of the GoM.

### 4.2.1 Freshwater inputs from the Atchafalaya–Mississippi River system and their interactions with LCE Olympus

Several studies of the coastal area adjacent to the Mississippi River (Boyle et al., 1984; Shiller and Boyle, 1991; Joung and Shiller, 2016; Shiller, 1993; Wen et al., 2011) and the West Florida shelf (WFS in Figure 4B; Mellett and Buck, 2020) have reported conspicuous coastal enrichment and the conservative behavior of dCu. Similarly, our study of the open water sites revealed high dCu (and cdom) concentrations, and a clear and inverse correlation with $S_A$ at the south of LCE Olympus (blue dots in Figures 4B–D, 5A, B), suggesting a fluvial source of dCu in this area. Satellite-derived distributions of SSS and the geostrophic velocity field during XIXIMI-4 provide additional support for this interpretation and support a strong interaction between LCE Olympus and the freshwater plume from the Mississippi River (Figure 4A; See also Brokaw et al (2019) and da Silva and Castelao (2018)). First, the lowest satellite-derived salinities and $S_A$ values together with the highest cdom concentrations were observed at stations A7 and A8

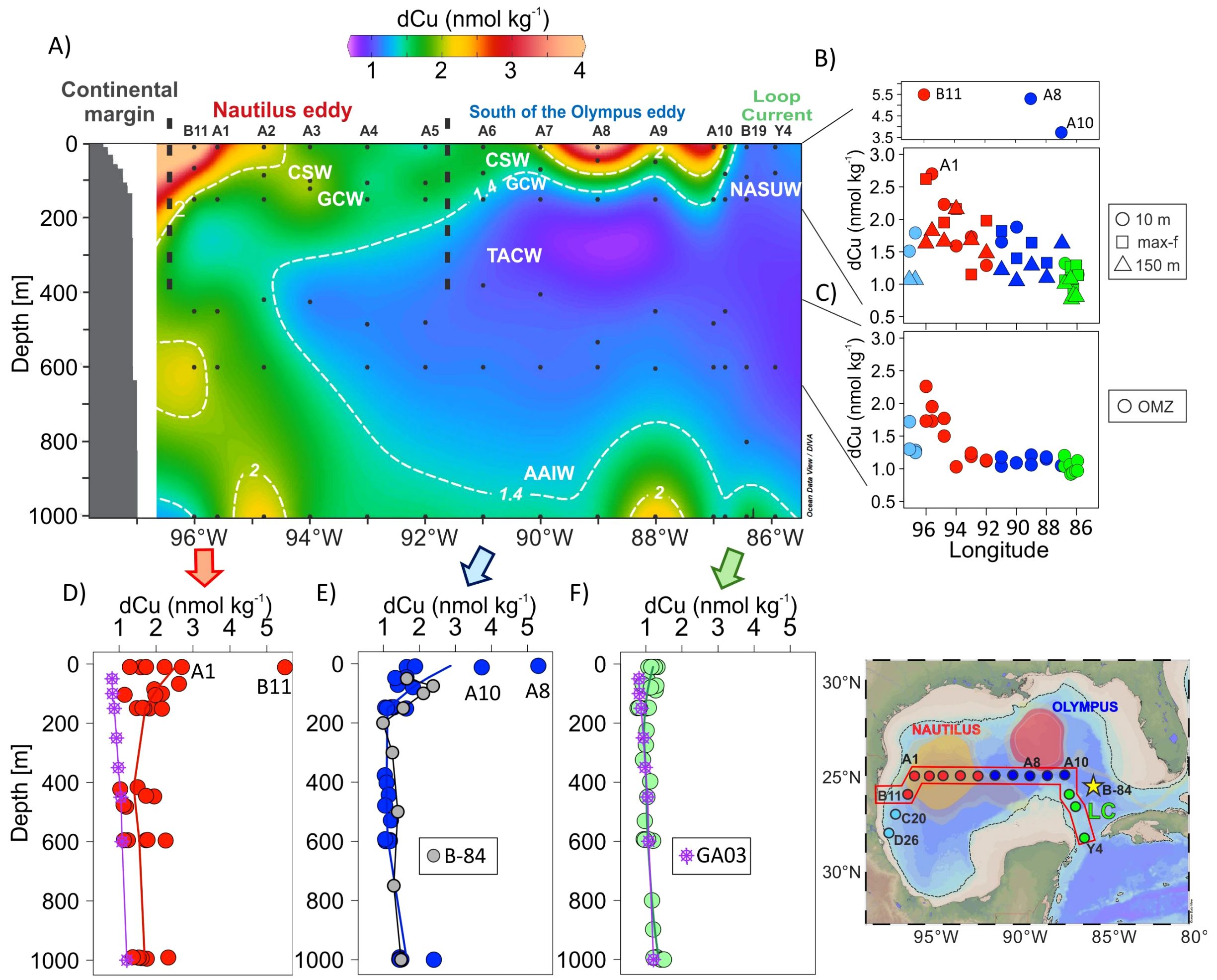


FIGURE 3
**(A)** Sectional distribution of dissolved copper (dCu; color scale) along the transect from the eastern coast of Mexico to the Yucatan Channel. The positions of the sampling stations are shown at the top, and the black vertical dashed lines show the approximate extension of the Loop Current Eddy (LCE) Nautilus. Acronyms for water masses as in Figure 2. **(B)** dCu concentrations vs. longitude along the transect at depths of 10 m (10-m), maximum fluorescence (max-f), 150 m (150-m), and **(C)** the oxygen minimum zone (OMZ). Vertical profiles of dCu for **(D)** LCE Nautilus (red circles), **(E)** south of LCE Olympus (blue circles along 25° N), and **(F)** Loop Current (green circles). For comparison, the average profile of dCu (purple stars) reported for the tropical North Atlantic during the GA03 cruise (Roshan and Wu, 2015) is shown in panels **(D, F)**, whereas the only vertical profile of dCu reported for the Loop Current (gray circles, B-84) is shown in panel **(E)**. The yellow star in the map of the Gulf of Mexico indicates the station (24°10′ N, 84°49′ W) sampled by Boyle et al. (1984). Note the dCu enrichment throughout the water column in the western section of the GoM. The map and sectional distribution of dCu shown in **(A)** were generated with Ocean Data View (Schlitzer, 2024).

in the central GoM (Figures 4A, C, D, 5A, B). Second, the satellite images also revealed that the surface currents at the northern edge of LCE Olympus trapped freshwater and transported it along the periphery on the eastern side of the eddy into the open water region of the GoM, more than 400 km from the Mississippi River Delta. This result is not surprising, as other authors have reported similar observations (e.g., Jochens and DiMarco, 2008; Morey et al., 2003; Yuan et al., 2004) and, more recently, others have modeled and captured in their simulations a southward flux of freshwater due to the interaction of the Mississippi River plume with the Loop Current and its mesoscale eddies (Bracco et al., 2019; Liu et al., 2022; Sun et al., 2022). The year 2015 was a particularly anomalous, with above-average freshwater discharge from the Mississippi River (Otis et al., 2019). This condition increased the extent of the freshwater plume over the continental shelf in the northern GoM (da Silva and Castelao, 2018), which was combined with a northward extension of the Loop Current (Brokaw et al., 2019; Otis et al., 2019). Consequently, during the summer of 2015, the newly detached LCE Olympus approached the Louisiana-Texas continental shelf, recirculating low-salinity water into the deep region of the GoM (Brokaw et al., 2019), further supporting our findings.

### 4.2.2 Conservative behavior of dCu in surface waters south of the LCE Olympus and its relationship with cdom

Terrestrial runoff is a major source of cdom in estuarine environments (Osburn et al., 2019) and studies in the coastal waters of the northern Gulf of Mexico have shown that cdom distribution is an effective tracer of salinity (Chaichitehrani et al.,

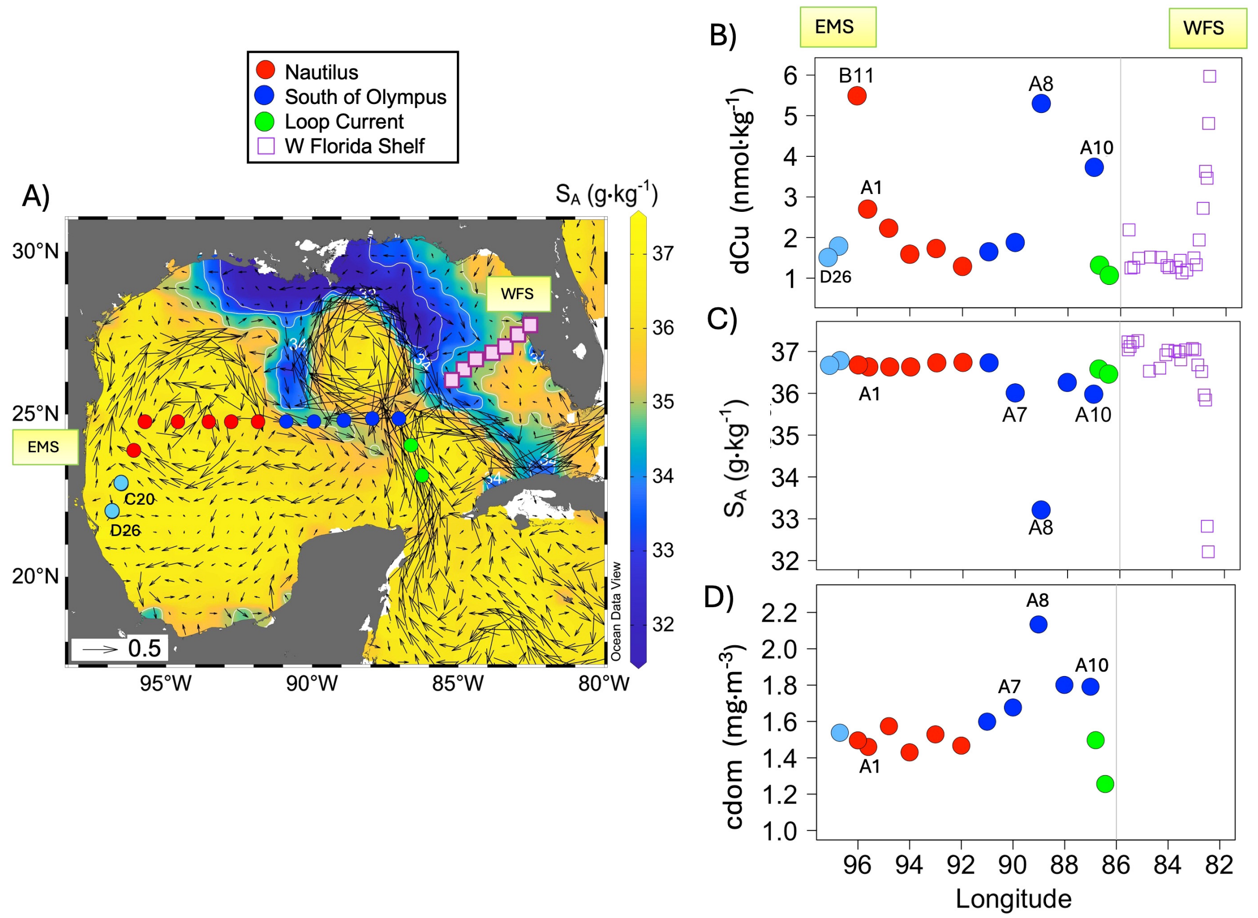


FIGURE 4
**(A)** Spatial distribution of satellite-derived sea surface salinity (SSS: color scale) and mean satellite-derived geostrophic velocity field (m $s^{-1}$) from 27 August 2015 to 3 September 2015. Longitudinal profiles of **(B)** the concentration of dissolved copper (dCu), **(C)** absolute salinity ($S_A$), and **(D)** chromophoric dissolved organic matter (cdom) at 10 m depth along a transect from the Eastern Mexican shelf (EMS; this study) to the West Florida shelf (WFS). The samples for dCu concentration and salinity from the WFS (purple squares) were collected in June 2015 and reported by Mellett and Buck (2020). The stations in all panels are colored as follows: Loop Current (LC; green circles), south of Loop Current Eddy (LCE) Olympus (blue circles along 25° N), LCE Nautilus (red circles). The labels next to the symbols show the station identifiers. The figure in panel **(A)** was generated with Ocean Data View (Schlitzer, 2024).

2014; Chen and Hu, 2017). Consistent with these findings, Figure 5B reveals that during the XIXIMI-4 campaign a negative correlation (r = -0.82, p<0.05) was observed between $S_A$ and cdom, indicating a riverine origin of cdom. Additionally, we found a positive correlation between cdom and dCu (r =0.64, p<0.05; Figure 5C) and, with the exception of station A10, the mixing diagram indicated that dCu exhibited conservative behavior in the lower-salinity region of our transect (Figure 5A); that is, the dCu concentration can be explained by the mixing of freshwater from the northern coast of the GoM and seawater originating in the Loop Current. This lack of dCu reactivity in the central gulf with freshwater influence, could be attributed to the strong complexation of Cu by organic ligands and the conservative dilution of the organic complexes (Shiller and Boyle, 1991; Shiller, 1993; Mellett and Buck, 2020; Wen et al., 2011). In estuarine systems dominated by riverine inputs of terrestrially derived compounds, a fraction of these compounds exhibits a strong capacity to complex Cu (e.g., Shank et al., 2004; Xue and Sigg, 1993). This condition is particularly relevant in coastal environments with low residence times as the transfer of Cu from strongly binding dissolved moieties to particles can be kinetically hindered (Achterberg et al., 2002); consequently, complexation by strong binding ligands may facilitate the rapid mobilization of dCu out of the system (Shank et al., 2004). Thus, given the intense dynamics and the conservative behavior of dCu in the northern coastal zone of the gulf (Shiller and Boyle, 1991; Joung and Shiller, 2016; Wen et al., 2011), we propose that, when combined with the rapid off-shelf transport driven by the rotational motion of the LCEs (e.g., Olympus), 1) the signal of freshwater and dCu inputs from the northern coastal zone can persist in offshore surface waters over distances spanning hundreds of kilometers; 2) the spatial variability of dCu-rich freshwater patches transported offshore by eddies is reflected in the increased spatial variability of surface dCu concentrations (Figures 3B, 4B); and is also indicative that 3) dCu is a good tracer of the signal of estuarine waters in the open water region of the GoM. However, for this last conclusion to hold, it is

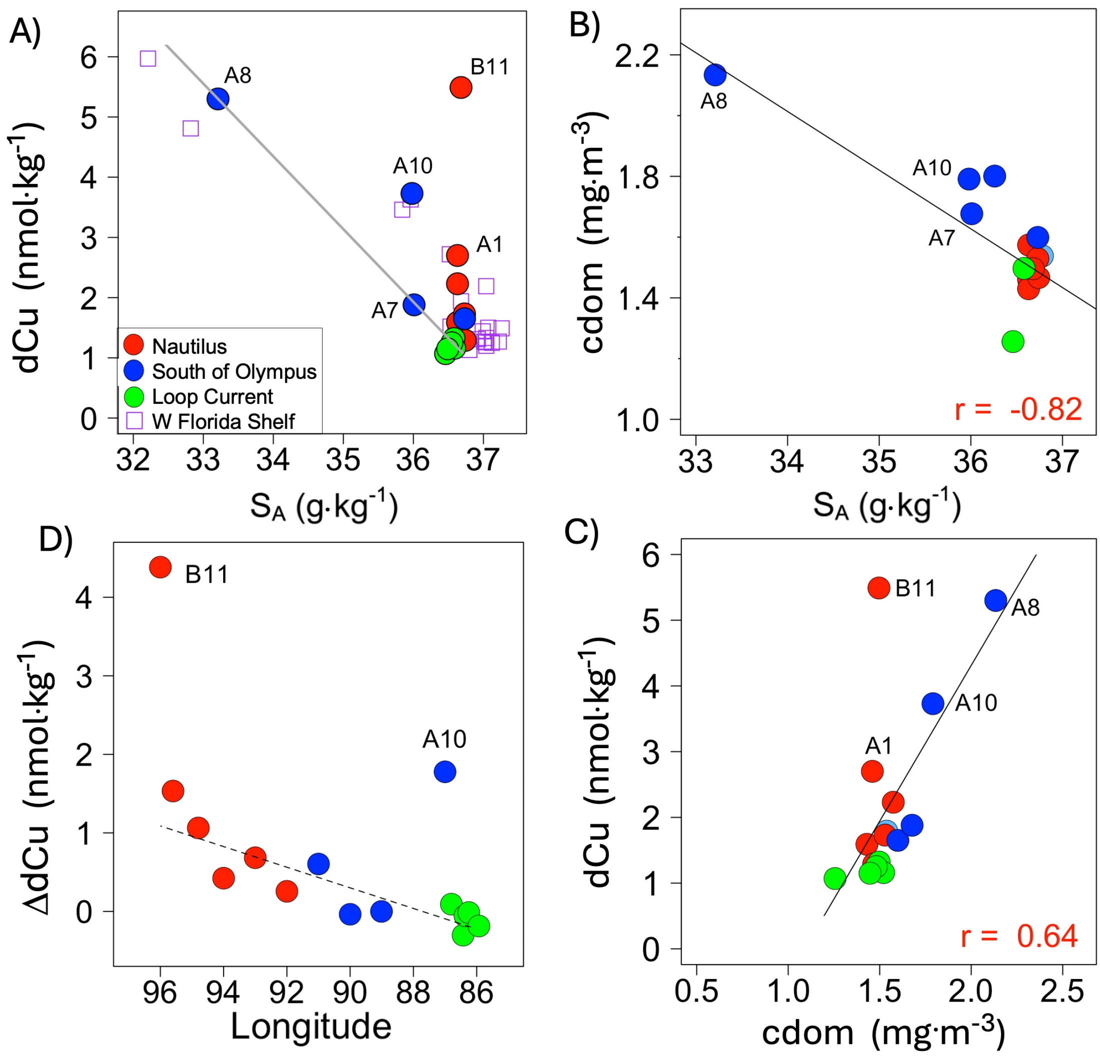


FIGURE 5
Distribution of **(A)** dissolved copper (dCu) and **(B)** chromophoric dissolved organic matter (cdom) as a function of absolute salinity ($S_A$) at 10 m depth along the transect during the XIXIMI-4 cruise. In panel **(A)**, a simple mixing model was used to predict the dCu concentrations that resulted from the mixing of freshwater from the Mississippi-Atchafalaya River system with seawater from the Loop Current. Data from the West Florida shelf (WFS) (purple squares; Mellett and Buck, 2020) are shown for comparison and were not used in the mixing model calculation. **(C)** Longitudinal profile of the concentration of non-conservative dCu (ΔdCu) at 10 m depth along the transect from the eastern coast of Mexico to the Yucatan Channel. The ΔdCu concentration at each station was calculated as $\Delta dCu = dCu_{measured} - dCu_{mixing}$, where $dCu_{mixing}$ is the dCu concentration predicted by the line of mixing at the $S_A$ measured at each station. The dashed line in **(D)** was included to indicate the westward spatial trend. **(D)** Relationship between surface dCu and cdom along the transect. The labels next to the symbols in all panels represent the station identifiers.

essential to demonstrate that the spatial variability of dCu is governed by physical dynamics and that exhibits conservative behavior within the system.

## 4.3 The non-conservative behavior of dCu in surface waters of the deep-water region of the GoM

Notably, if all surface samples of the transect were considered, the mixing diagram indicated that the relationship between dCu and salinity in the deep-water region increased in complexity (Figure 5A). That is, the surface concentration of dCu in some stations (e.g., A1, A10, and B11) could not be explained by simple mixing between freshwater and seawater from the Loop Current. This suggests that other biogeochemical processes or external supplies may also be responsible. Generally, the signals of biogeochemical processes or external dCu inputs in a mixing diagram are detected as deviations from linearity (e.g., Waeles et al., 2005; Mellett and Buck, 2020). Processes such as scavenging and biological uptake reduce metal concentrations in seawater, resulting in negative deviations, while processes like the remineralization of organic matter, benthic fluxes, fluvial inputs, and atmospheric deposition increase metal concentrations, leading to positive deviations. Thus, the non-conservative fraction of copper (ΔdCu) in surface waters was particularly high in stations B11 (4.38

nmol·kg$^{-1}$) and A10 (1.78 nmol·kg$^{-1}$). Overall, the spatial distribution of this fraction tended to increase towards the LCE Nautilus (Figure 5D), revealing the existence of high values of ΔdCu in the western portion of the GoM. In the case of A10, which was located to the south of LCE Olympus, and stations A1 and B11, which were located within LCE Nautilus, fluvial inputs from the continent could not explain the excess dCu given that it was not associated with a decrease in $S_A$ at the surface (Figures 5A, 4B, C). Therefore, other external sources that could supply Cu in sufficient quantities are needed to explain its enrichment in the surface waters of the gulf, such as the inputs of soluble Cu from atmospheric deposition of dust or sedimentary inputs from the continental margin.

## 4.4 Atmospheric deposition of soluble Cu to the GoM

Atmospheric particles originate from diverse sources, including desert regions, the burning of biomass, and anthropogenic emissions (e.g., Mahowald et al., 2018). Following their deposition, the influence of these particles on the composition of seawater depends on several factors, such as their chemical composition and grain size, atmospheric processing, and sea surface temperature (Baker et al., 2006; Félix-Bermúdez et al., 2020; Sedwick et al., 2007). The trade winds are known to carry large quantities of dust particles from the Sahara Desert (Chiapello et al., 1995) across the Atlantic Ocean to the GoM each summer (Ebling and Landing, 2017; Hayes et al., 2022; Lenes et al., 2001, Lenes et al., 2012; Prospero, 1999). Thus, the high surface concentrations of dCu recorded in the western GoM might be due to the atmospheric deposition from this transatlantic source. In a study conducted in the summer of 2015, two months before XIXIMI-4, Mellett and Buck (2020) measured the surface concentration of dCu along a transect on the western coast of the Florida shelf (Figure 4B). These authors suggested that Saharan dust deposition may have contributed to elevating the offshore total dissolvable concentration of Cu in surface waters in the Loop Current area of their transect.

Thus, to deduce the origin of the atmospheric particles that arrived to the GoM during XIXIMI-4, we calculated five-day AMBTs (Stein et al., 2015) and analyzed the spatial distribution of AOD in the region, including the Atlantic Ocean. The AMBT arrival heights of 100 m and 500 m indicated that the first four days of the cruise (27–30 August 2015) were not "typical" summer days, given that the air masses present at the time of sampling had previously crossed the continental region of North America (Figures 6A, B). After passing the region of LCE Nautilus as the ship moved eastward (31 August 2015 to 3 September 2015), the AMBTs began to follow the dominant pattern of the Easterly trade winds during summer (Figures 6A, B). In support of this result, the AOD observations of 26–31 August 2015 indicated that the distribution of aerosol particles over the surrounding continental region was dominated by air masses that transported aerosols from North America (Figures 6C, D). Although the distribution of AOD and AMBT alone cannot indicate where particles were incorporated into the trajectory of the air mass (Stuut et al., 2005), this analysis suggests that the elevated dCu concentrations at the surface in the western portion of LCE Nautilus (stations A1 and B11) were potentially the result of atmospheric deposition. To test whether this idea was correct, we quantified the increase in the dCu concentration (δdCu) due to the flux of soluble Cu associated with mineral and anthropogenic atmospheric particle deposition using Equation 1:

$$\boldsymbol{\delta dCu} = \frac{(F_{atm-Cu} \times FS_{Cu} \times \tau)}{(h \times \rho)} \tag{1}$$

where $F_{\text{atm-Cu}}$ is the total atmospheric flux of Cu, $FS_{\text{Cu}}$ is the fractional solubility of Cu in atmospheric particles, τ is the retention time of water in the zone, $h$ is the depth, and ρ is the density of seawater. Taking from the literature a range of total Cu flux of 8–39 nmol·m$^{-2}$·d$^{-1}$ (Ebling and Landing, 2017) for the GoM, an $FS_{\text{Cu}}$ value of 0.17 for mineral dust and a value of 0.76 for anthropogenic aerosols (López-García et al., 2017; Sholkovitz et al., 2010), a water retention time in anticyclonic eddies in the northwestern GoM of 4 weeks (Bello-Fuentes et al., 2021), a surface water density of 1024 kg·m$^{-3}$, and a depth of 10 m, the dCu concentration in our study area would increase between 4 and 81 pmol·kg$^{-1}$. An aeolian flux of soluble Cu of that magnitude would only explain between 0.2% (mineral dust deposition) and 3.4% (anthropogenic aerosol deposition) of the average (± se) non-conservative dCu fraction (2.32 ± 1.04 nmol·kg$^{-1}$) in the top 10 m of the water column in the region of LCE Nautilus. In the same way, a significant enrichment of Cu in dust particles would be necessary for their flux to contribute substantially to the excess dCu in the GoM. For instance, to supply at least 50% of the observed non-conservative dCu (1.16 nmol·kg$^{-1}$), continuous deposition of aerosols (13.7 mg·m$^{-2}$·d$^{-1}$; Hayes et al., 2022) over one month would require a total Cu concentration of 41.9 μmol·g$^{-1}$ (69 times higher than the upper crustal average of 0.61 μmol·g$^{-1}$; Li and Schoonmaker, 2003) and a high solubility (74% characteristic of anthropogenic particles) in the upper 10 m of the water column (density=1024 kg·m$^{-3}$). Such Cu-enriched aerosols (particles ≤10 μm) have been reported in industrialized coastal cities such as Tampico, Tamaulipas, on the eastern coast of Mexico (22 μmol·g$^{-1}$; Flores-Rangel et al., 2014) and Houston, Texas, on the Gulf coast of USA (1–14 μmol·g$^{-1}$; Bozlaker et al., 2013). However, due to the summer atmospheric circulation in the GoM, it is unlikely that a constant, large-scale offshore flux of such enriched particles to the region can be sustained. Therefore, the results of this quantitative exercise indicated that the atmospheric supply of soluble Cu played a minor role during the summer of 2015 and, consequently, an additional source must be considered to explain the excess dCu in this sector of the GoM.

## 4.5 Dissolved Cu enrichment and the impact of LCE Nautilus in the western region of the GoM

Figure 3B shows that dCu clearly increased from the Loop Current towards LCE Nautilus in the upper 150 m of the water

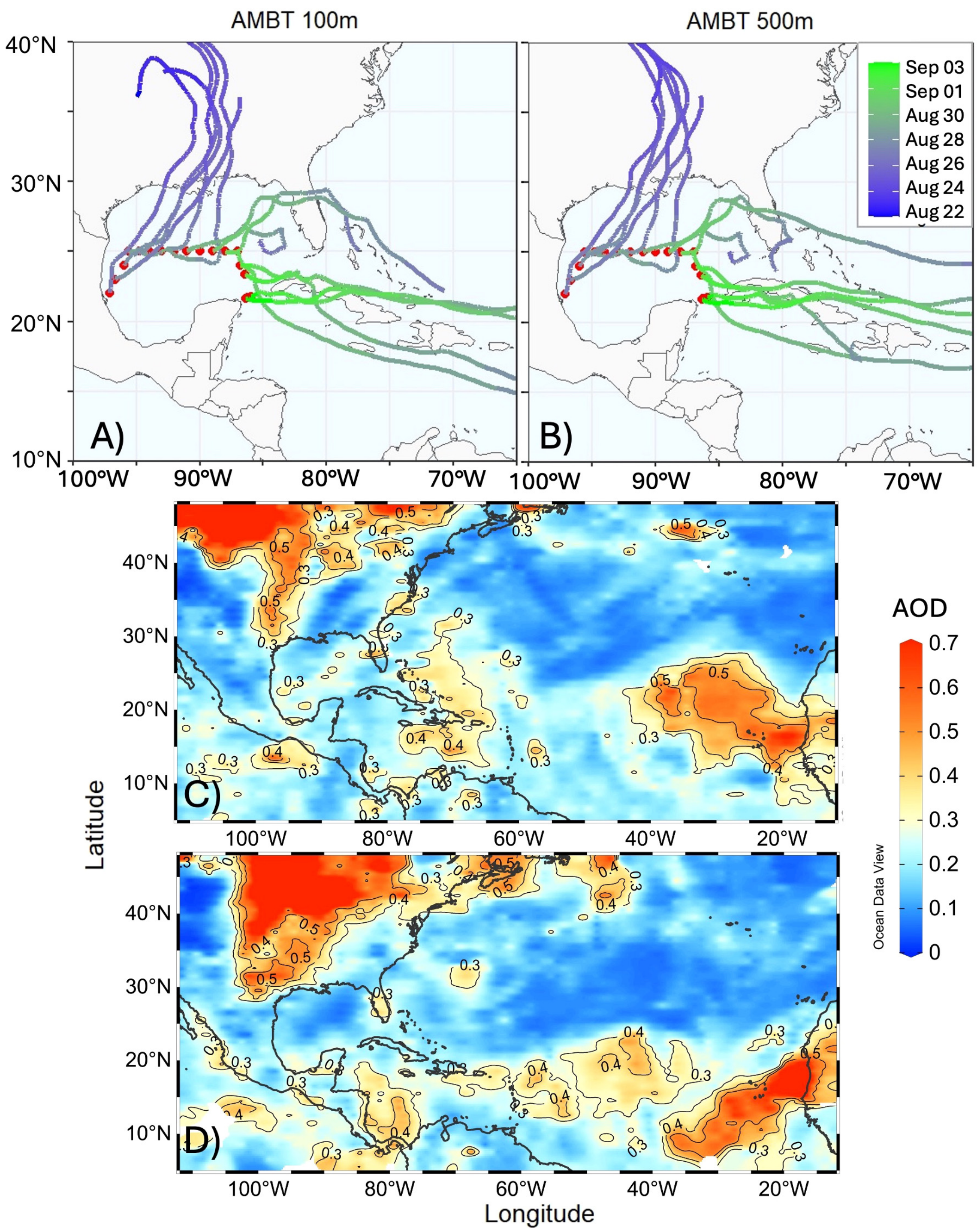


FIGURE 6
Five-day air mass back-trajectories (AMBTs) derived from the HYSPLIT model for the period of 22 August 2015 to 3 September 2015 (color scale). Red circles in panels A-B represent the sampling stations along the transect during the first leg of the XIXIMI-4 cruise. AMBTs were computed for all stations with an ending height of **(A)** 100 m and **(B)** 500 m above sea level. Spatial composites of the aerosol optical depth (AOD) over the Gulf of Mexico (GoM) and Atlantic Ocean from the NASA MODIS-A satellite at 550 nm averaged over the period of **(C)** 26 August to 28 August and **(D)** 29 August to 31 August.

column, which cannot be explained by the atmospheric deposition of Cu, as discussed in section 4.4. Notably, the high dCu levels observed at the surface in stations B11 and A1 within the LCE Nautilus were linked to elevated salinities and reduced cdom concentrations (Figures 2B, C, 4B–D), which attest against the possibility of significant freshwater influence in the western region of the Gulf. Similarly, when comparing dCu content in the different water masses in the upper 150 m of the water column, dCu was higher in the western GoM than in the Yucatan Channel (Table 1). For example, the average dCu values in CSW (1.97 ± 0.53 nmol·kg$^{-1}$) and GCW (1.75 ± 0.26 nmol·kg$^{-1}$) in the region of LCE Nautilus were significantly higher than those in CSW (1.12 ± 0.14 nmol·kg$^{-1}$) and NASUW (0.95 ± 0.19 nmol·kg$^{-1}$) in the region of the Loop Current. This increase in dCu could not have come from the area south of LCE Nautilus because the dCu values at stations C20 and D26 in the upper 150 m of the water column were much lower than those in the eddy stations (Figure 3B). In addition, the increase in dCu could not have come from the northern coastal zone of LCE Nautilus because the eddy was rotating clockwise (Figure 4A) nor could it have come from below, given that isopycnals deepen within anticyclones (Figure 2B; Supplementary Figure S1A). Thus, with this downward vertical transport characteristic of anticyclones, dCu would have moved towards the bottom. Therefore, the increase in dCu in the western GoM indicates that the supply of dCu originated in the adjacent continental shelf (Figure 3A). This result agrees with those of previous reports for other marginal regions of the ocean that have reported increases in dCu in areas near the continental shelf (e.g., Bruland, 1980; Kremling, 1985; Pohl et al., 2011; Roshan and Wu, 2015), which has been generally attributed to benthic fluxes. Similarly, in the GoM (Boyle et al., 1984; Lenstra et al., 2022) and other marginal seas (e.g., Heggie et al., 1987; Vieira et al., 2019; Seo et al., 2022), it has been suggested that sediments are important sources of Cu -and other trace metals such as Mn, Fe, Co, Ni- to the overlying waters. In oxic environments, Cu can be released from the sediments by the aerobic respiration of organic matter or through the biologically mediated reductive dissolution of Cu-bearing Fe/Mn oxyhydroxides in suboxic sediments (Hines et al., 1984; Posacka et al., 2017). Thus, we suggest that the benthic dCu flux is responsible for the excess observed in the first 150 m of the water column in the westernmost stations in the region of LCE Nautilus and that this flux of dCu occurs due to the remineralization of organic matter in shelf sediments.

However, to sustain the dCu gradient between the shelf and the open sea, a flow from the continental shelf that introduces dCu along the isopycnals is required. We propose that mesoscale eddies may contribute to the formation and maintenance of this dCu gradient given that 1) they can persist coherent for several weeks before dissipating along the western coast of the GoM (Bello-Fuentes et al., 2021; Tenreiro et al., 2018); 2) when colliding with the shelf, the currents parallel to the coast reach velocities >1 $m \cdot s^{-1}$ (Dubranna et al., 2011; Zavala-Hidalgo et al., 2003; Gómez-Valdivia and Parés-Sierra, 2020); 3) these currents have the capacity to transport large volumes of water away from the shelf (Guerrero et al., 2020; Hamilton et al., 2015). However, the magnitude of water exchange depends on several factors such as the proximity, shape, and angle of orientation of the anticyclones with respect to the continental shelf (Guerrero et al., 2020). These authors also reported that offshore transport was greater at the northern edge of the LCEs impinging on the western margin of the gulf, while the greatest inshore transport occurred at their southern edge, which is consistent with our results for the summer of 2015. The spatial distribution of geostrophic currents (Figure 4A) indicated that once LCE Nautilus approached the coastal region, the currents to the west of the eddy moved parallel to the coast and subsequently turned eastward, carrying water from the shelf towards the open sea. Thus, this water exchange mechanism between the continental shelf and the central region of the gulf, along with a sedimentary source of dCu, would explain the east-west dCu gradient reported in this work. Previous studies on dCu distribution in surface waters of the GoM have identified a consistent pattern of decreasing dCu concentrations from nearshore to open waters off Louisiana-Mississippi (Boyle et al., 1984; Shiller and Boyle, 1991; Wen et al., 2011) and the West Florida Shelf (Mellett and Buck, 2020). These studies attributed the source of dCu to freshwater inputs from North America. Similarly, our findings reveal a well-defined gradient of dCu concentrations decreasing from west to east. However, we show that the source of dCu in this region originates due to the interaction between the sediments and the colliding LCEs eddies that promote enhanced off-shelf transport along the western coast. Altogether, these findings reveal the existence of distinct mechanisms that shape the dCu distribution in the open waters of the GoM and underscore the complexity of the biogeochemical cycle of Cu in the GoM, which will require further data to be fully understood.

## 4.6 Benthic release of dCu in the OMZ and its relationship with LCE Nautilus

The OMZ is an environment with low levels of dissolved oxygen in subsurface waters, which is characteristic of TACW in the western Atlantic. This layer penetrates the GoM (e.g., Quintanilla et al., 2024) and was present throughout our transect from the LC in the east to the continental slope on the west coast (Figure 2D). Figure 3 shows that the dCu concentrations at depths of 400–600 m in the OMZ were generally uniform ($x = 1.10 \pm 0.08$ $nmol \cdot kg^{-1}$) from the Loop Current to station A3 (Figures 3A, C). Thus, on a net basis, dCu was neither added nor removed from this isopycnal layer ($\sigma_t = 27.18 \pm 0.11$ $kg \cdot m^{-3}$) during its journey of more than 750 km into the GoM (Figures 3A, C). This apparent stability of dCu could indicate that there is a balance between scavenging and remineralization of Cu (Roshan and Wu, 2015) or, alternatively, it might be attributed to the slow regeneration of Cu associated with organic matter in the water column of the gulf (Hollister et al., 2020). Similar observations have been reported for the open-ocean OMZ of the Eastern Tropical North Atlantic (Roshan and Wu, 2015) and Eastern Tropical South Pacific (Jacquot et al., 2013; Roshan and Wu, 2018). It has been argued that dCu is not affected by oxygen-poor waters, suggesting that the respiration of organic matter in the OMZ of these ecosystems plays a minor role. However, once LCE Nautilus reached the near-slope zone, the dCu concentration in the OMZ notably increased in stations A2, A1, and B11 ($1.82 \pm 0.26$ $nmol \cdot kg^{-1}$; Figures 3A, C), representing a 75% increase relative to the average dCu value in the Loop Current at the same depth. This dCu enrichment in the OMZ may be partially explained by the remineralization of organic matter in the water column or by a signal derived from the sediments (e.g., denitrification and the reductive dissolution of Mn/Fe oxides; Beckler et al., 2016; Owings et al., 2021). The difference between these sources can be approximated by considering that TACW moves from the Loop Current towards the western GoM (Quintanilla et al., 2024) and solving the following mass balance along the potential density anomaly ($27.18 \pm 0.11$ $kg \cdot m^{-3}$), we have Equation 2:

$$dCu_w - dCu_{LC} = \Delta Cu_{Rem} + \Delta Cu_{Bent} \tag{2}$$

where $dCu_w$ and $dCu_{LC}$ represent the concentration of dCu in the region of LCE Nautilus and the Loop Current, respectively, and $\Delta Cu_{Rem}$ and $\Delta Cu_{Bent}$ are the increase in dCu associated with the remineralization of organic matter in the water column and benthic flux, respectively. Given that $\Delta Cu_{Rem}$ can be estimated from the change in apparent oxygen utilization (AOU) during its journey from the Loop Current to the slope of western GoM, we can obtain the sedimentary flux using Equations 3 and 4:

$$\Delta Cu_{Bent} = dCu_w - dCu_{LC} - \Delta Cu_{Rem} \tag{3}$$

$$\Delta Cu_{Bent} = dCu_w - dCu_{LC} - (AOU_w - AOU_{LC}) \times \left[\frac{C}{O}\right]_{Redfield} \times \left[\frac{Cu}{C}\right]_{Phyto} \tag{4}$$

where $[\frac{C}{O}]_{Redfield}$ is the Redfield ratio of C/O and $[\frac{Cu}{C}]_{Phyto}$ is the Cu/C ratio in organic matter of phytoplanktonic origin. Thus, considering a $[\frac{Cu}{C}]_{Phyto}$ value of 0.011 nmol·µmol$^{-1}$ (Richon and Tagliabue, 2019; Twining and Baines, 2013) and our average values of $dCu_w$, $dCu_{LC}$, $AOU_w$, and $AOU_{LC}$ in the layer of 400–600 m in the region of the Loop Current and western portion of LCE Nautilus (A1, A2, and B11), $\Delta Cu_{Rem}$ and $\Delta Cu_{Bent}$ values of 0.043 nmol·kg$^{-1}$ and 0.737 nmol·kg$^{-1}$ are obtained, respectively. These results imply that sediment input is primarily responsible (95%) for dCu enrichment in the OMZ in the western GoM, with remineralization of organic matter in the water column only contributing a minor fraction (~5%). These findings align with previous studies on the OMZs of the Eastern Tropical North Atlantic (Roshan and Wu, 2015) and the Eastern Tropical South Pacific (Jacquot et al., 2013; Roshan and Wu, 2018). These studies reported that water column remineralization has a negligible net effect on the subsurface distribution of dCu and highlighted that slope sediments contribute to copper enrichment in the water column near the continental slope. However, in the case of the GoM, a physical mechanism is required to resuspend sediments from continental slope and dCu release from interstitial waters into the water column. While purely diffusive fluxes could also introduce dCu from interstitial waters, physical resuspension could greatly amplify inputs and introduce particles as well, with this latter process eventually leading to delayed inputs of Cu from desorption. We propose that the dynamics of mesoscale eddies (Dubranna et al., 2011; Guerrero et al., 2020; Hamilton et al., 2015) interacting with the slope provide the energy necessary for diagenetic remobilization and the transport of dCu of sedimentary origin (Figure 3A) away from the substrate where it was released.

Finally, two processes have been presented in the literature to explain the tendency of dCu to increase with respect to depth in the ocean: 1) reversible scavenging, which involves the dissolution of Cu in particles that are transported to the sea floor (Little et al., 2013; Richon and Tagliabue, 2019), and 2) the benthic flux of dCu into the water column (Boyle et al., 1977, Boyle et al, 1984; Klinkhammer et al., 1982; Liang et al., 2023; Roshan and Wu, 2015; Roshan et al., 2020; Takano et al., 2014). While further research is needed to provide quantitative data, particularly on reversible scavenging (Cui and Gnanadesikan, 2022), our findings support the hypotheses that sediments are a significant source of this element in the GoM and that physical processes, such as mesoscale eddies, can recycle dCu and modify its vertical distribution in subsurface waters.

## 5 Conclusions

This paper presents the distribution of dCu in the upper 1000 m of the water column in a quasi-zonal transect (25° N) in the deep-water region of the GoM during the summer of 2015. The joint impact of mesoscale dynamics and external inputs (fluvial, sedimentary, and aeolian inputs) on the spatial distribution of this trace element in this marginal sea is highlighted. In the region of the Loop Current, the dCu profiles were similar to those of the Atlantic Ocean, which reflects the origin of the water entering the GoM. The concentration of dCu in surface waters along the transect was highly variable and, in part, due to the interaction between LCE Olympus and the freshwater inputs from the Mississippi River with relatively high dCu content. During 2015, freshwater fluxes in the northern coastal region of the GoM were above average and LCE Olympus exhibited a greater northern extent, making this year rather unique. These conditions favored greater and faster off-shelf transport due to the rotational motion of LCE Olympus, which resulted in the signal of dCu and freshwater inputs from the northern coastal zone of the gulf to be observed hundreds of kilometers away in central GoM. Thus, we suggest that dCu is an effective tracer that may be used to identify the influence of water of estuarine origin in the open water region of the GoM. Additionally, we identified a clear dCu gradient in surface waters, with dCu increasing from the Loop Current to the region of LCE Nautilus. The vertical dCu profiles in the region of LCE Nautilus exhibited the highest concentrations, which were significantly higher than those of the Atlantic Ocean. This dCu enrichment in the western GoM was attributed to higher off-shelf transport promoted by the decay of LCE Nautilus and benthic inputs from the continental shelf and slope, with atmospheric inputs at the surface and organic matter remineralization in the water column playing minor roles. Based on our results, anticyclonic eddies that have detached from the Loop Current and that interact or collide with the continental shelf and slope of the GoM are capable of trapping dCu-rich water from the coastal zone and transporting it to the deep-water region of the GoM. Thus, the interaction of the LCEs with the continental shelf and slope constitutes a mechanism of water exchange between the coastal zone and the deep-water region that is capable of modifying and shaping the spatial distribution of dCu within this marginal sea.

## Data availability statement

The original contributions presented in the study are included in the article/Supplementary Material. Further inquiries can be directed to the corresponding author.

## Author contributions

FD-H: Conceptualization, Data curation, Formal analysis, Funding acquisition, Investigation, Visualization, Writing – original draft, Writing – review & editing, Supervision. AF-B: Data curation, Investigation, Software, Visualization, Writing – review & editing, Methodology, Validation. ET-D: Data curation, Methodology, Project administration, Writing – review & editing, Validation. MH-D: Funding acquisition, Investigation, Writing – review & editing. ML: Conceptualization, Funding acquisition, Investigation, Methodology, Project administration, Resources, Writing – review & editing. AT-S: Data curation, Methodology, Resources, Writing – review & editing, Validation. SQ-D-O: Investigation, Visualization, Writing – review & editing, Conceptualization, Methodology. MR-B: Data curation, Methodology, Visualization, Writing – review & editing.

## Funding

The author(s) declare that financial support was received for the research and/or publication of this article. This research was funded by the Mexican National Council for Science and Technology - Mexican Ministry of Energy-Hydrocarbon Fund [project number 201441]. This is a contribution of the Gulf of Mexico Research Consortium (CIGoM). We acknowledge PEMEX's specific request to the Hydrocarbon Fund to address the environmental effects of oil spills in the Gulf of Mexico. Support in the form of graduate scholarships awarded to M.R-B. and S.Q.-O. by the Mexican National Council for Science and Technology (CONACYT), is greatly acknowledged.

## Acknowledgments

The authors thank the chief scientist Dr. S.Z. Herzka and scientific party as well as captain and crew of R/V Justo Sierra during the XIXIMI-4 cruise for their valuable help and support during sampling at sea. We express our gratitude to E. Gutierrez for her contribution to sample processing during analysis and to D. Sanchez-Quiles for his assistance in the dissolved Cu analysis by ICP-MS at the ICMAN-CSIC facilities. Aqua-MODIS AOD presented in this work was obtained from the Giovanni online data system maintained by the NASA Goddard Earth Sciences. The authors gratefully acknowledge the NOAA Air Resources Laboratory (ARL) for the provision of the HYSPLIT transport and dispersion model used in this paper. We also extend our gratitude to both reviewers for their helpful suggestions and critical comments, which improved the quality of this article. English translation by Andrea Liévana MacTavish is gratefully acknowledged. FDH dedicates this work to Dr. Alberto Zirino, an outstanding mentor and friend.

## Conflict of interest

The authors declare that the research was conducted in the absence of any commercial or financial relationships that could be construed as a potential conflict of interest.

The author(s) declared that they were an editorial board member of Frontiers, at the time of submission. This had no impact on the peer review process and the final decision.

## Generative AI statement

The author(s) declare that no Generative AI was used in the creation of this manuscript.

## Publisher's note

All claims expressed in this article are solely those of the authors and do not necessarily represent those of their affiliated organizations, or those of the publisher, the editors and the reviewers. Any product that may be evaluated in this article, or claim that may be made by its manufacturer, is not guaranteed or endorsed by the publisher.

## Supplementary material

The Supplementary Material for this article can be found online at: https://www.frontiersin.org/articles/10.3389/fmars.2025.1551655/full#supplementary-material

## References

Achterberg, E. P., Van Elteren, J. T., and Kolar, Z. I. (2002). Species kinetics and heterogeneous reactivity of dissolved Cu in natural freshwaters. *Environ. Sci. Technol.* 36, 914–920. doi: 10.1021/es010109m

Arnone, V., Santana-Casiano, J. M., Gonzalez-Davila, M., Planquette, H., Sarthou, G., Gerringa, L. J. A., et al. (2023). Natural copper-binding ligands in the Arctic Ocean. The influence of the Transpolar Drift (GEOTRACES GN04). *Front. Mar. Sci.* 10. doi: 10.3389/fmars.2023.1306278

Baker, A. R., Jickells, T. D., Witt, M., and Linge, K. L. (2006). Trends in the solubility of iron, aluminium, manganese and phosphorus in aerosol collected over the Atlantic Ocean. *Mar. Chem.* 98, 43–58. doi: 10.1016/j.marchem.2005.06.004

Beckler, J. S., Kiriazis, N., Rabouille, C., Stewart, F. J., and Taillefert, M. (2016). Importance of microbial iron reduction in deep sediments of river-dominated continental-margins. *Mar. Chem.* 178, 22–34. doi: 10.1016/j.marchem.2015.12.003

Bello-Fuentes, F. J., Garcia-Nava, H., Andrade-Canto, F., Durazo1, R., Castro1, R., and Yarbuh, I. (2021). Retention time and transport potential of eddies in the northwestern Gulf of Mexico. *Cienc. Mar* 47, 71–88. doi: 10.7773/cm.v47i2.3116

Boyle, E. A., Reid, D. F., Huested, S. S., and Hering, J. (1984). Trace metals and radium in the Gulf of Mexico: an evaluation of river and continental shelf sources. *Earth Planet. Sci. Lett.* 69, 69–87. doi: 10.1016/0012-821X(84)90075-X

Boyle, E. A., Sclater, F. R., and Edmond, J. M. (1977). The distribution of dissolved copper in the Pacific. *Earth Planet. Sci. Lett.* 37, 38–54. doi: 10.1016/0012-821X(77)90144-3

Bozlaker, A., Buzcu-Güven, B., Fraser, M. P., and Chellam, S. (2013). Insights into PM10 sources in Houston, Texas: Role of petroleum refineries in enriching lanthanoid metals during episodic emission events. *Atmospheric Environ.* 69, 109–117. doi: 10.1016/j.atmosenv.2012.11.068

Bozlaker, A., Prospero, J. M., Price, J., and Chellam, S. (2019). Identifying and quantifying the impacts of advected north african dust on the concentration and composition of airborne fine particulate matter in houston and galveston, texas. *J. Geophys. Res. Atmos* 124, 12282–12300. doi: 10.1029/2019JD030792

Bracco, A., Liu, G., and Sun, D. (2019). Mesoscale-submesoscale interactions in the Gulf of Mexico: from oil dispersion to climate. *Chaos Solitons Fractals* 119, 63–72. doi: 10.1016/j.chaos.2018.12.012

Brokaw, R. J., Subrahmanyam, B., and Morey, S. L. (2019). Loop current and eddy-driven salinity variability in the Gulf of Mexico. *Geophys. Res. Lett.* 46, 5978–5986. doi: 10.1029/2019GL082931

Bruland, K. W. (1980). Oceanographic distributions of cadmium, zinc, nickel, and copper in the North Pacific. *Earth Planet. Sci. Lett.* 47, 176–198. doi: 10.1016/0012-821X(80)90035-7

Bruland, K. W., Franks, R. P., Knauer, G. A., and Martin, J. H. (1979). Sampling and analytical methods for the determination of copper, cadmium, zinc, and nickel at the nanogram per liter level in sea water. *Anal. Chim. Acta* 105, 233–245. doi: 10.1016/S0003-2670(01)83754-5

Bruland, K. W., Middag, R., and Lohan, M. C. (2014). "Controls of trace metals in seawater," in *Treatise on geochemistry: second edition*, *2nd ed.*Eds. H. D. Holland and K. K. Turekian (Oxford: Elsevier Ltd), 19–51. doi: 10.1016/B978-0-08-095975-7.00602-1

Buck, C. S., Hammerschmidt, C. R., Bowman, K. L., Gill, G. A., and Landing, W. M. (2015). Flux of total mercury and methylmercury to the northern Gulf of Mexico from US estuaries. *Environ. Sci. Technol.* 49, 13992–13999. doi: 10.1021/acs.est.5b03538

Candela, J., Ochoa, J., Sheinbaum, J., López, M., Pérez-Brunius, P., Tenreiro, M., et al. (2019). The flow through the gulf of Mexico. *J. Phys. Oceanogr.* 49, 1381–1401. doi: 10.1175/jpo-d-18-0189.1

Candela, J., Sheinbaum, J., Ochoa, J., Badan, A., and Leben, R. (2002). The potential vorticity flux through the Yucatan Channel and the Loop Current in the Gulf of Mexico. *Geophys. Res. Lett.* 29, 2059. doi: 10.1029/2002GL015587

Chaichitehrani, N., D'Sa, E. J., Ko, D. S., Walker, N. D., Osburn, C. L., and Chen, R. F. (2014). Colored dissolved organic matter dynamics in the northern Gulf of Mexico from ocean color and numerical model results. *J. Coastal Res.* 30, 800–814. doi: 10.2112/JCOASTRES-D-13-00036.1

Chen, S., and Hu, C. (2017). Estimating sea surface salinity in the northern Gulf of Mexico from satellite ocean color measurements. *Remote Sens. Environ.* 201, 115–132. doi: 10.1016/j.rse.2017.09.004

Chiapello, I., Bergametti, G., Gomes, B., and Chatenet, B. (1995). An additional low layer transport of Sahelian and Saharan dust over the north-eastern tropical Atlantic. *Geophys. Res. Lett.* 22, 3191–3194. doi: 10.1029/95GL03313

Cui, M., and Gnanadesikan, A. (2022). Characterizing the roles of biogeochemical cycling and ocean circulation in regulating marine copper distributions. *J. Geophys. Res. Oceans* 127, 1–20. doi: 10.1029/2021JC017742

Cutter, G., Casciotti, K., Croot, P., Geibert, W., Heimbürger, L. E., Lohan, M., et al. (2017). *Sampling and sample-handling protocols for GEOTRACES cruises. version 3* (Toulouse: GEOTRACES International Project Office). doi: 10.25607/OBP-2

da Silva, C. E., and Castelao, R. M. (2018). Mississippi river plume variability in the Gulf of Mexico from SMAP and MODIS-Aqua observations. *J. Geophys. Res. Oceans* 123, 6620–6638. doi: 10.1029/2018JC014159

Daudén-Bengoa, G., Sheinbaum, J., RodríguezOuterelo, J., and Herzka, S. Z. (2024). Coupling of potential habitat models with particle tracking experiments to examine larval fish dispersal and connectivity in deep water regions. *PloS One* 19, e0308357. doi: 10.1371/journal

Delgadillo-Hinojosa, F., Macías-Zamora, J. V., Segovia-Zavala, J. A., and Torres-Valdés, S. (2001). Cadmium enrichment in the gulf of california. *Mar. Chem.* 75, 109–122. doi: 10.1016/S0304-4203(01)00028-7

Delgadillo-Hinojosa, F., Segovia-Zavala, J. A., Huerta-Díaz, M. A., and Atilano-Silva, H. (2006). Influence of geochemical and physical processes on the vertical distribution of manganese in Gulf of California waters. *Deep Sea Res. Part I Oceanogr. Res. Pap.* 53, 1301–1319. doi: 10.1016/j.dsr.2006.06.002

Diercks, A. R., Dike, C., Asper, V. L., DiMarco, S. F., Chanton, J. P., and Passow, U. (2018). Scales of seafloor sediment resuspension in the northern Gulf of Mexico. *Elementa: Sci. Anthropocene* 6, 1–28. doi: 10.1525/elementa.285

Draxler, R. R., and Hess, G. D. (1998). An overview of the HYSPLIT_4 modelling system for trajectories, dispersion, and deposition. *Aust. Meteorol. Mag.* 47, 295–308.

Dubranna, J., Pérez-Brunius, P., López, M., and Candela, J. (2011). Circulation over the continental shelf of the western and southwestern Gulf of Mexico. *J. Geophys. Res.* 116, C08009. doi: 10.1029/2011JC007007

Ebling, A. M., and Landing, W. M. (2017). Trace elements in the sea surface microlayer: rapid responses to changes in aerosol deposition. *Elem Sci. Anth* 5, 42. doi: 10.1525/elementa.237

Elliott, B. A. (1982). Anticyclonic rings in the gulf of Mexico. *J. Phys. Ocean* 12, 1292–1309. doi: 10.1175/1520-0485(1982)012<1292:ARITGO>2.0.CO;2

Félix-Bermúdez, A., Delgadillo-Hinojosa, F., Lares, M. L., Torres-Delgado, E. V., Huerta-Díaz, M. A., Tovar-Sanchez, A., et al. (2023). Spatial variability of dissolved nickel is enhanced by mesoscale dynamics in the Gulf of Mexico. *Front. Mar. Sci.* 9. doi: 10.3389/fmars.2022.1036331

Félix-Bermúdez, A., Delgadillo-Hinojosa, F., Torres-Delgado, E. V., and Muñoz-Barbosa, A. (2020). Does sea surface temperature sffect solubility of iron in mineral dust? The Gulf of California as a case study. *J. Geophys. Res. Oceans* 125, 1–18. doi: 10.1029/2019JC015999

Flores-Rangel, R. M., Rodríguez-Espinosa, P. F., de Oca-Valero, J. A. M., Mugica-alvarez, V., Ortiz-Romero-Vargas, M. E., Navarrete-López, M., et al. (2014). Temporal variation of PM10 and metal concentrations in Tampico, Mexico. *Air Quality Atmosphere Health* 8, 367–378. doi: 10.1007/s11869-014-0291-6

Gaillardet, J., Viers, J., and Dupré, B. (2014). "Trace elements in river waters," in *Treatise on geochemistry: second edition*. Eds. H. D. Holland and K. K. Turekian (Amsterdam: Elsevier), 195–236. doi: 10.1016/B978-0-08-095975-7.00507-6

Gierach, M. M., Vazquez-Cuervo, J., Lee, T., and Tsontos, V. M. (2013). Aquarius and SMOS detect effects of an extreme Mississippi River flooding event in the Gulf of Mexico. *Geophys. Res. Lett.* 40, 5188–5193. doi: 10.1002/grl.50995

Gómez-Valdivia, F., and Parés-Sierra, A. (2020). Seasonal upper shelf circulation along the central western gulf of Mexico: A preferential upcoast flow reinforced by the recurrent arrival of loop current eddies. *J. Geophys. Res. Oceans* 125, e2019JC015596. doi: 10.1029/2019jc015596

Guerrero, L., Sheinbaum, J., Mariño-Tapia, I., Gonzalez-Rejón, J. J., and Pérez-Brunius, P. (2020). Influence of mesoscale eddies on cross-shelf exchange in the western Gulf of Mexico. *Cont. Shelf Res.* 209, 104243. doi: 10.1016/j.csr.2020.104243

Hamilton, P., Fargion, G., and Biggs, D. (1999). Loop Current eddy paths in the western Gulf of Mexico. *J. Phys. Oceanogr.* 29, 1180–1207. doi: 10.1175/15200485(1999)029<1180:LCEPIT>2.0.CO;2

Hamilton, P., Leben, R., Bower, A., Furey, H., and Pérez-Brunius, P. (2018). Hydrography of the Gulf of Mexico using autonomous floats. *J. Phys. Oceanogr.* 48, 773–794. doi: 10.1175/JPO-D-17-0205.1

Hamilton, P., Speer, K., Snyder, R., Wienders, N., and Leben, R. R. (2015). Shelf break exchange events near the de soto canyon. *Cont. Shelf Res.* 110, 25–38. doi: 10.1016/j.csr.2015.09.021

Hayes, C. T., Shiller, A. M., and Milroy, S. P. (2022). Toward constraining sources of lithogenic metals in the northern Gulf of Mexico. *J. Geophys. Res. Oceans* 127, e2022JC018523. doi: 10.1029/2022JC018523

Heggie, D., Klinkhammer, G., and Cullen, D. (1987). Manganese and copper fluxes from continental margin sediments. *Geochim. Cosmochim. Acta* 51, 1059–1070. doi: 10.1016/0016-7037(87)90200-6

Hines, M. E., Lyones, W. M. B., Armstrong, P. B., Orem, W. H., Spencer, M. J., and Gaudette, H. E. (1984). Seasonal metal remobilization in sediments of Great Bay, New Hampshire. *Mar. Chem.* 15, 173–178. doi: 10.1016/0304-4203(84)90014-8

Hollister, A. P., Kerr, M., Malki, K., Muhlbach, E., Robert, M., Tilney, C. L., et al. (2020). Regeneration of macronutrients and trace metals during phytoplankton decay: An experimental study. *Limnol. Oceanogr.* 65, 1936–1960. doi: 10.1002/lno.11429

Hu, C., Nelson, J. R., Johns, E., Chen, Z., Weisberg, R. H., and Müller-Karger, F. E. (2005). Mississippi River water in the Florida Straits and in the Gulf Stream off Georgia in summer 2004. *Geophys. Res. Lett.* 32, 1–5. doi: 10.1029/2005GL022942

Jacquot, J. E., Kondo, Y., Knapp, A. N., and Moffett, J. W. (2013). The speciation of copper across active gradients in nitrogen-cycle processes in the eastern tropical South Pacific. *Limnol. Oceanogr.* 58, 1387–1394. doi: 10.4319/lo.2013.58.4.1387

Jacquot, J. E., and Moffett, J. W. (2015). Copper distribution and speciation across the International GEOTRACES Section GA03. *Deep Sea Res. Part II Top. Stud. Oceanogr.* 116, 187–207. doi: 10.1016/j.dsr2.2014.11.013

Jochens, A. E., and DiMarco, S. F. (2008). Physical oceanographic conditions in the deepwater gulf of Mexico in summer 2000–2002. *Deep Sea Res. Part II Top. Stud. Oceanogr.* 55, 2541–2554. doi: 10.1016/j.dsr2.2008.07.003

Jordi, A., Basterretxea, G., Tovar-Sanchez, A., Alastuey, A., and Querol, X. (2012). Copper aerosols inhibit phytoplankton growth in the Mediterranean Sea. *Proc. Natl. Acad. Sci. U.S.A.* 109, 21246–21249. doi: 10.1073/pnas.1207567110

Joung, D., Guo, L., and Shiller, A. M. (2019). Role of the Atchafalaya River Basin in regulating export fluxes of dissolved organic carbon, nutrients, and trace elements to the Louisiana Shelf. *J. Hydrol. X* 2, 100018. doi: 10.1016/j.hydroa.2019.100018

Joung, D. J., and Shiller, A. M. (2016). Temporal and spatial variations of dissolved and colloidal trace elements in Louisiana Shelf waters. *Mar. Chem.* 181, 25–43. doi: 10.1016/j.marchem.2016.03.003

Kenlee, B., Owens, J. D., Raiswell, R., Poulton, S. W., Severmann, S., Sadler, P. M., et al. (2024). Long-range transport of dust enhances oceanic iron bioavailability. *Front. Mar. Sci.* 11. doi: 10.3389/fmars.2024.1428621

Klinkhammer, G., Heggie, D. T., and Graham, D. W. (1982). Metal diagenesis in oxic marine sediments. *Earth Planet. Sci. Lett.* 61, 211–219. doi: 10.1016/0012-821X(82)90054-1

Kremling, K. (1985). The distribution of cadmium, copper, nickel, manganese, and aluminium in surface waters of the open Atlantic and European shelf area. *Deep Sea Res. Part I Oceanogr. Res. Pap.* 32, 531555. doi: 10.1016/0198-0149(85)90043-3

La Fontaine, S., Quinn, J. M., Nakamoto, S. S., Dudley Page, M., Moseley, G.V., Kropat, J., et al. (2002). Copper-dependent iron assimilation pathway in the model photosynthetic eukaryote Chlamydomonas reinhardtii. *Eukaryotic Cell* 1, 736–757. doi: 10.1128/EC.1.5.736-757.2002

Leben, R. R. (2005). Altimeter-derived loop current metrics. *Geophys. Monogr. Ser.* 161, 181–201. doi: 10.1029/161GM15

Lee-Sanchez, E., Camacho-Ibar, V. F., Velasquez-Aristizabal, J. A., Valencia-Gasti, J. A., and Samperio-Ramos, G. (2022). Impacts of mesoscale eddies on the nitrate distribution in the deep-water region of the Gulf of Mexico. *J. Mar. Syst.* 229, 1–19. doi: 10.1016/j.jmarsys.2022.103721

Lenes, J. M., Darrow, B. P., Cattrall, C., Heil, C. A., Callahan, M., Vargo, G. A., et al. (2001). Iron fertilization and the Trichodesmium response on the West Florida shelf. *Limnol. Oceanogr.* 46, 1261–1277. doi: 10.4319/lo.2001.46.6.1261

Lenes, J. M., Prospero, J. M., Landing, W. M., Virmani, J. I., and Walsh, J. J. (2012). A model of Saharan dust deposition to the eastern Gulf of Mexico. *Mar. Chem.* 134–135, 1–9doi: 10.1016/j.marchem.2012.02.007

Lenstra, W. K., van Helmond, N. A. G. M., Żygadłowska, O. M., van Zummeren, R., Witbaard, R., and Slomp, C. P. (2022). Sediments as a source of iron, manganese, cobalt and nickel to continental shelf waters (Louisiana, Gulf of Mexico). *Front. Mar. Sci.* 9. doi: 10.3389/fmars.2022.811953

Li, Y. H., and Schoonmaker, J. E. (2003). "7.01 - chemical composition and mineralogy of marine sediments," in *Treatise on geochemistry*. Eds. D. H. Henriech and K. T. Karl (Pergamon, Oxford), 1–35.

Liang, H., Moffett, J. W., and John, S. G. (2023). Toward a better understanding of the global ocean copper distribution and speciation through a data-constrained model. *Global Biogeochemical Cycles* 37, e2023GB007769. doi: 10.1029/2023GB007769

Linacre, L., Durazo, R., Camacho-Ibar, V. F., Selph, K. E., Lara-Lara, J. R., Mirabal-Gomez, U., et al. (2019). Picoplankton carbon biomass assessments and distribution of prochlorococcus ecotypes linked to loop current eddies during summer in the southern gulf of Mexico. *J. Geophys. Res. Ocean.* 124, 8342–8359. doi: 10.1029/2019JC015103

Little, S. H., Vance, D., Siddall, M., and Gasson, E. (2013). A modeling assessment of the role of reversible scavenging in controlling oceanic dissolved Cu and Zn distributions. *Global Biogeochemical Cycles* 27, 780–791. doi: 10.1002/gbc.20073

Liu, G., Bracco, A., and Sun, D. (2022). Offshore freshwater pathways in the northern gulf of Mexico: impacts of modeling choices. *Front. Mar. Sci.* 9. doi: 10.3389/fmars.2022.841900

López-García, P., Gelado-Caballero, M. D., Collado-Sanchez, C., and Hernandez-Brito, J. J. (2017). Solubility of aerosol trace elements: Sources and deposition fluxes in the Canary Region. *Atmospheric Environ.* 148, 167–174. doi: 10.1016/j.atmosenv.2016.10.035

Mahowald, N. M., Hamilton, D. S., Mackey, K. R. M., Moore, J. K., Baker, A. R., Scanza, R. A., et al. (2018). Aerosol trace metal leaching and impacts on marine microorganisms. *Nat. Commun.* 9, 2614. doi: 10.1038/s41467-018-04970-7

Maldonado, M. T., Allen, A. E., Chong, J. S., Lin, K., Leus, D., Karpenko, N., et al. (2006). Copper-dependent iron transport in coastal and oceanic diatoms. *Limnol. Oceanogr.* 51 (4), 1729–1743. doi: 10.4319/lo.2006.51.4.1729

Mallick, D., Wang, X., and Beebe, D. A. (2022). Impact of estuaries on fluvial Cr input into the ocean: Perspectives from the Mobile Bay Estuary, Northern Gulf of Mexico. . *Geochimica Cosmochimica Acta* 334, 187–200. doi: 10.1016/j.gca.2022.08.004

Mann, E. L., Ahlgren, N., Moffett, J. W., and Chisholm, S. W. (2002). Copper toxicity and cyanobacterial ecology in the Sargasso Sea. *Limnol. Oceanogr.* 47, 976–988. doi: 10.4319/lo.2002.47.4.0976

Manta, G., Durante, G., Candela, J., Send, U., Sheinbaum, J., Lankhorst, M., et al. (2023). Predicting the Loop Current dynamics combining altimetry and deep flow measurements through the Yucatan Channel. *Front. Mar. Sci.* 10. doi: 10.3389/fmars.2023.1156159

McDougall, T. J., and Barker, P. M. (2011). *Getting started with TEOS–10 and the Gibbs Seawater (GSW) oceanographic toolbox.* 28ISBN: 978–0-646–55621-5, SCOR/IAPSO WG127. Available at: www.TEOS-10.org.

Mellett, T., and Buck, K. N. (2020). Spatial and temporal variability of trace metals (Fe, Cu, Mn, Zn, Co, Ni, Cd, Pb), iron and copper speciation, and electroactive Fe-binding humic substances in surface waters of the eastern Gulf of Mexico. *Mar. Chem.* 227, 1–15. doi: 10.1016/j.marchem.2020.103891

Metcalfe, S. E., Barron, J. A., and Davies, S. J.. (2015). The Holocene history of the North American Monsoon: 'known knowns' and 'known unknowns' in understanding its spatial and temporal complexity. *Quat. Sci. Rev.* 120, 1–27. doi: 10.1016/j.quascirev.2015.04.004

Meunier, T., Pallas-Sanz, E., Tenreiro, M., Portela, E., Ochoa, J., Ruiz-Angulo, A., et al. (2018). The vertical structure of a loop current eddy. *J. Geophys. Res. Ocean.* 123, 6070–6090. doi: 10.1029/2018JC013801

Meunier, T., Pallas Sanz, E., de Marez, C., Pérez, J., Tenreiro, M., Ruiz-Angulo, A., et al. (2021). The dynamical structure of a warm core ring as inferred from glider observations and along-Track Altimetry. *Remote Sens.* 13, 2456. doi: 10.3390/rs13132456

Moffett, J. W., and Zika, R. G. (1988). Measurement of copper (I) in surface waters of the subtropical Atlantic and Gulf of Mexico. *Geochim. Cosmochim. Acta* 52, 1849–1857. doi: 10.1016/0016-7037(88)90008-7

Morey, S. L., Martin, P. J., O'Brien, J. J., Wallcraft, A. A., and Zavala-Hidalgo, J. (2003). Export pathways for river discharged fresh water in the northern Gulf of Mexico. *J. Geophys. Res.* 108, 3303. doi: 10.1029/2002JC001674

Muller-Karger, F. E., Smith, J. P., Werner, S., Chen, R., Roffer, M., Liu, Y., et al. (2015). Natural variability of surface oceanographic conditions in the offshore Gulf of Mexico. *Prog. Oceanogr.* 134, 54–76. doi: 10.1016/j.pocean.2014.12.007

Osburn, C. L., Margolin, A. R., Guo, L., Bianchi, T. S., and Hansell, D. A. (2019). Dissolved, colloidal, and particulate organic matter in the Gulf of Mexico. Chapter 7. In "*Gulf of Mexico Origin, Waters, and Biota: Volume 5, Chemical Oceanography*": T. S. Bianchi (ed.). ISBN-10: 1623497744. Texas A&M University Press, 294pp.

Otis, D., Le Hénaff, M., Kourafalou, V., McEachron, L., and Muller-Karger, F. (2019). Mississippi River and Campeche Bank (Gulf of Mexico) episodes of cross-shelf export of coastal waters observed with satellites. *Remote Sens.* 11, 723. doi: 10.3390/rs11060723

Owings, S. M., Bréthous, L., Eitel, E. M., Fields, B. P., Boever, A., Beckler, J. S., et al. (2021). Differential manganese and iron recycling and transport in continental margin sediments of the Northern Gulf of Mexico. *Mar. Chem.* 229, 103908. doi: 10.1016/j.marchem.2020.103908

Patricola, C. M., Hansen, G. E., and Sena, A. C. T. (2024). The influence of climate variability and future climate change on atlantic hurricane season length. *Geophys. Res. Lett.* 51, e2023GL107881. doi: 10.1029/2023gl107881

Paytan, A., Mackey, K. R. M., Chen, Y., Lima, I. D., Doney, S. C., Mahowald, N., et al. (2009). Toxicity of atmospheric aerosols on marine phytoplankton. *Proc. Natl. Acad. Sci. U.S.A.* 106, 4601–4605. doi: 10.1073/pnas.0811486106

Peers, G., and Price, N. M. (2006). Copper-containing plastocyanin used for electron transport by an oceanic diatom. *Nature* 441, 341–344. doi: 10.1038/nature04630

Peers, G., Quesnel, S.-A., and Price, N. M. (2005). Copper requirements for iron acquisition and growth of coastal and oceanic diatoms. *Limnol. Oceanogr.* 50, 1149–1158. doi: 10.4319/lo.2005.50.4.1149

Pérez-Brunius, P., Furey, H., Bower, A., Hamilton, P., Candela, J., García-Carrillo, P., et al. (2018). Dominant circulation patterns of the deep Gulf of Mexico. *J. Phys. Oceanogr.* 48, 511–529. doi: 10.1175/JPO-D-17-0140.1

Pohl, C., Croot, P. L., Hennings, U., Daberkow, T., Budeus, G., and Loeff, M. R. V. D. (2011). Synoptic transects on the distribution of trace elements (Hg, Pb, Cd, Cu, Ni, Zn, Co, Mn, Fe, and Al) in surface waters of the northern- and southern east Atlantic. *J. Mar. Syst.* 84, 28–41. doi: 10.1016/j.jmarsys.2010.08.003

Portela, E., Tenreiro, M., Pallàs-Sanz, E., Meunier, T., Ruiz-Angulo, A., Sosa-Gutiérrez, R., et al. (2018). Hydrography of the central and western gulf of Mexico. *J. Geophys. Res. Oceans* 123, 1–16. doi: 10.1029/2018JC013813

Posacka, A. M., Semeniuk, D. M., Whitby, H., van den Berg, C. M. G., Cullen, J. T., Orians, K., et al. (2017). Dissolved copper (dCu) biogeochemical cycling in the subarctic Northeast Pacific and a call for improving methodologies. *Mar. Chem.* 196, 47–61. doi: 10.1016/j.marchem.2017.05.007

Prospero, J. M. (1999). Long-term measurements of the transport of African mineral dust to the southeastern United States: Implications for regional air quality. *J. Geophys. Res.* 104, 15917–15927. doi: 10.1029/1999JD900072

Prospero, J. M., Glaccum, R. A., and Nees, R. T. (1981). Atmospheric transport of soil dust from Africa to South America. *Nature* 289, 570–572. doi: 10.1038/289570a0

Quintanilla, J. G., Herguera, J. C., and Sheinbaum, J. (2024). Oxygenation of the Gulf of Mexico thermocline linked to the detachment of Loop Current Eddies. *Front. Mar. Sci.* 11. doi: 10.3389/fmars.2024.1479837

R Core Team (2024). *A language and environment for statistical computing* (Vienna, Austria: R Foundation for Statistical Computing). Available at: https://www.R-project.org/.

Ren, X., Luke, W. T., Kelley, P., Cohen, M., Ngan, F., Artz, R., et al. (2014). Mercury speciation at a coastal site in the northern Gulf of Mexico: Results from the Grand Bay intensive studies in summer 2010 and spring 2011. *Atmosphere* 5, 230–251. doi: 10.3390/atmos5020230

Richon, C., and Tagliabue, A. (2019). Insights into the major processes driving the global distribution of copper in the ocean from a global model. *Global Biogeochemical Cycles* 33, 1594–1610. doi: 10.1029/2019GB006280

Roshan, S., DeVries, T., and Wu, J. (2020). Constraining the global ocean Cu cycle with a data-assimilated diagnostic model. *Global Biogeochemical Cycles* 34, 1–15. doi: 10.1029/2020GB006741

Roshan, S., and Wu, J. (2015). The distribution of dissolved copper in the tropical-subtropical north Atlantic across the GEOTRACES GA03 transect. *Mar. Chem.* 176, 189–198. doi: 10.1016/j.marchem.2015.09.006

Roshan, S., and Wu, J. (2018). Dissolved and colloidal copper in the tropical South Pacific. *Geochim. Cosmochim. Acta* 233, 81–94. doi: 10.1016/j.gca.2018.05.008

Ruacho, A., Richon, C., Whitby, H., and Bundy, R. M. (2022). Sources, sinks, and cycling of dissolved organic copper binding ligands in the ocean. *Commun. Earth Environ.* 3, 263. doi: 10.1038/s43247-022-00597-

Schlitzer, R. (2024). *Ocean data view*. Available online at: https://odv.awi.de (Accessed December 14, 2024).

Schmitz, W. J., and McCartney, M. S. (1993). On the north atlantic circulation. *Rev. Geophys.* 31, 29–49. doi: 10.1029/92RG02583

Scott, S. R., Dunion, J. P., Olson, M. L., and Gay, D. A. (2022). Lead isotopes in North American precipitation record the presence of Saharan dust. *Bull. Am. Meteorol. Soc* 103, E281–E292. doi: 10.1175/BAMS-D-20-0212.1

Sedwick, P. N., Sholkovitz, E. R., and Church, T. M. (2007). Impact of anthropogenic combustion emissions on the fractional solubility of aerosol iron: Evidence from the Sargasso Sea. *Geochemistry Geophysics Geosystems* 8, n/a–n/a. doi: 10.1029/2007gc001586

Segovia-Zavala, J. A., Delgadillo-Hinojosa, F., and Alvarez-Borrego, S. (1998). Cadmium in the coastal upwelling area adjacent to the california – Mexico border. *Estuar. Coast. Shelf Sci.* 46, 475–481. doi: 10.1006/ecss.1997.0296

Segovia-Zavala, J. A., Lares, M. L., Delgadillo-Hinojosa, F., Tovar-Sanchez, A., and Sañudo-Wilhelmy, S. A. (2010). Dissolved iron distributions in the central region of the Gulf of California, México. *Deep Sea Res. Part I Oceanogr. Res. Pap.* 57, 53–64. doi: 10.1016/j.dsr.2009.10.007

Seo, H., Kim, G., Kim, T., Kim, I., Ra, K., and Jeong, H. (2022). Trace elements (Fe, Mn, Co, Cu, Cd, and Ni) in the East Sea (Japan Sea): Distributions, boundary inputs, and scavenging processes. *Mar. Chem.* 239(2022)104070. doi: 10.1016/j.marchem.2021.104070

Shank, G. C., Skrabal, S. A., Whitehead, R. F., and Kieber, R. J. (2004). Strong copper complexation in an organic-rich estuary: the importance of allochthonous dissolved organic matter. *Mar. Chem.* 88, 21–39. doi: 10.1016/j.marchem.2004.03.001

Shiller, A. M. (1993). Comparison of nutrient and trace element distributions in the delta and shelf outflow regions of the Mississippi and Atchafalaya Rivers. *Estuaries* 16, 541–546. doi: 10.2307/1352601

Shiller, A. M., and Boyle, E. A. (1991). Trace elements in the Mississippi River Delta outflow region: Behavior at high dis- charge. *Geochim. Cosmochim. Acta* 55, 3241–3251. doi: 10.1016/0016-7037(91)90486-O

Sholkovitz, E. R., Sedwick, P. N., and Church, T. M. (2010). On the fractional solubility of copper in marine aerosols: Toxicity of aeolian copper revisited. *Geophys. Res. Lett.* 37, 1–4. doi: 10.1029/2010GL044817

Stein, A. F., Draxler, R. R., Rolph, G. D., Stunder, B. J. B., Cohen, M. D., and Ngan, F. (2015). NOAA's hysplit atmospheric transport and dispersion modeling system. *Bull. Am. Meteorol. Soc* 96, 2059–2077. doi: 10.1175/BAMS-D-14-00110.1

Sturges, W., and Leben, R. (2000). Frequency of ring separations from the loop current in the gulf of Mexico: A revised estimate. *J. Phys. Oceanogr.* 30, 1814–1819. doi: 10.1175/1520-0485(2000)030<1814:FORSFT>2.0.CO;2

Stuut, J. B., Zabel, M., Ratmeyer, V., Helmke, P., Schefuß, E., Lavik, G., et al. (2005). Provenance of present-day eolian dust collected off NW Africa. *J. Geophys. Res.* 110, D04202. doi: 10.1029/2004JD005161

Sun, D., Bracco, A., and Liu, G. (2022). The role of freshwater forcing on surface predictability in the Gulf of Mexico. *J. Geophys. Res. Oceans* 127, e2021JC018098. doi: 10.1029/2021JC018098

Sunda, W. G., and Ferguson, R. L. (1983). "Sensitivity of natural bacterial communities to additions of copper and to cupric ion activity: a bioassay of copper complexation in seawater," in *Trace Metals in Seawater*, eds C. S. Wong, E. Boyle, K. W. Bruland, J. D. Burton and E. D. Goldberg (New York, NY: Plenum), 871–891.

Takano, S., Tanimizu, M., Hirata, T., and Sohrin, Y. (2014). Isotopic constraints on biogeochemical cycling of copper in the ocean. *Nat. Commun.* 5, 1–7. doi: 10.1038/ncomms6663

Tenreiro, M., Candela, J., Sanz, E. P., Sheinbaum, J., and Ochoa, J. (2018). Near-surface and deep circulation coupling in the western Gulf of Mexico. *J. Phys. Oceanogr.* 48, 145–161. doi: 10.1175/JPO-D-17-0018.1

Tong, D. Q., Gill, T. E., Sprigg, W. A., Van Pelt, R. S., Baklanov, A. A., Barker, B. M., et al. (2023). Health and safety effects of airborne soil dust in the Americas and beyond. *Rev. Geophys.* 61, e2021RG000763. doi: 10.1029/2021RG000763

Tovar-Sanchez, A. (2012). "Sampling approaches for trace elements determination in seawater," in *Comprehensive sampling and sample preparation*. Ed. J. Pawliszyn (Academic Press, Oxford), 317–334. doi: 10.1016/B978-0-12381373-2.00017-X

Twining, B. S., and Baines, S. B. (2013). The trace metal composition of marine phytoplankton. *Ann. Rev. Mar. Sci.* 5, 191–215. doi: 10.1146/annurev-marine-121211-172322

Valencia-Gasti, J. A., Camacho-Ibar, V. F., and Herguera, J. C. (2022). Water mass structure and mixing fractions in the deepwater region of the gulf of Mexico. *J. Geophys. Res. Oceans* 127, e2021JC017705. doi: 10.1029/2021jc017705

Vance, D., Archer, C., Bermin, J., Perkins, J., Statham, P. J., Lohan, M. C., et al. (2008). The copper isotope geochemistry of rivers and the oceans. *Earth Planet. Sci. Lett.* 274, 204–213. doi: 10.1016/j.epsl.2008.07.026

Vazquez-Cuervo, J., Fournier, S., Dzwonkowski, B., and Reager, J. (2018). Intercomparison of *in-situ* and remote sensing salinity products in the Gulf of Mexico, a river-influenced system. *Remote Sens.* 10, 1590 doi: 10.3390/rs10101590

Vidal, V. M., Vidal, F. V., Hernandez, A. F., Meza, E., and Zambrano, L. (1994). Winter water mass distributions in the western Gulf of Mexico affected by a colliding anticyclonic ring. *J. Oceanogr.* 50, 559–588. doi: 10.1007/BF02235424

Vidal, V. M., Vidal, F. V., and Perez-Molero, J. M. (1992). Collision of a loop current anticyclonic ring against the continental shelf slope of the western Gulf of Mexico. *J. Geophys. Res.* 97, 2155–2172. doi: 10.1029/91JC00486

Vieira, L. H., Achterberg, E. P., Scholten, J., Beck, A. J., Liebetrau, V., Mills, M. M., et al. (2019). Benthic fluxes of trace metals in the Chukchi Sea and their transport into the Arctic Ocean. *Mar. Chem.* 208, 43–55. doi: 10.1016/j.marchem.2018.11.001

Vukovich, F. M. (2007). Climatology of ocean features in the Gulf of Mexico using satellite remote sensing data. *J. Phys. Oceanogr.* 37, 689–707. doi: 10.1175/JPO2989.1

Vukovich, F. M., and Crissman, B. W. (1986). Aspects of warm rings in the Gulf of Mexico. *J. Geophys. Res.* 91, 2645–2660. doi: 10.1029/JC091iC02p02645

Waeles, M., Riso, R. D., and Le Corre, P. (2005). Seasonal variations of dissolved and particulate copper species in estuarine waters. *Estuar. Coast. Shelf Sci.* 62, 313–323. doi: 10.1016/j.ecss.2004.09.019

Wang, F. J., Chen, Y., Guo, Z. G., Gao, H. W., Mackey, K. R., Yao, X. H., et al. (2017). Combined effects of iron and copper from atmospheric dry deposition on ocean productivity. *Geophys. Res. Lett.* 44 (5), 2546–2555. doi: 10.1002/2016gl072349

Wen, L. S., Santschi, P. H., Warnken, K. W., Davison, W., Zhang, H., Li, H. P., et al. (2011). Molecular weight and chemical reactivity of dissolved trace metals (Cd, Cu, Ni) in surface waters from the Mississippi River to Gulf of Mexico. *Estuar. Coast. Shelf Sci.* 92, 649–658. doi: 10.1016/j.ecss.2011.03.009

Wong, K. H., Obata, H., Kim, T., Kondo, Y., and Nishioka, J. (2021). New insights into the biogeochemical cycling of copper in the subarctic Pacific: Distributions, size fractionation, and organic complexation. *Limnol. Oceanogr.* 66, 1424–1439. doi: 10.1002/lno.11695

Wu, J. T., and Lorenzen, H. (1984). Effect of copper on photosynthesis in synchronous Chlorella cells. *Bot. Bull. Academia Sin.* 25, 125–132.

Xue, H., and Sigg, L. (1993). Free cupric ion concentration and Cu (II) speciation in a eutrophic lake. *Limnol. Oceanogr* 38, 1200–1213. doi: 10.4319/lo.1993.38.6.1200

Yuan, J., Miller, R. L., Powell, R. T., and Dagg, M. J. (2004). Storm-induced injection of the Mississippi River plume into the open Gulf of Mexico. *Geophys. Res. Lett.* 31, L09312. doi: 10.1029/2003GL019335

Zavala-Hidalgo, J., Morey, S. L., and O'Brien, J. J. (2003). Seasonal circulation on the western shelf of the Gulf of Mexico using a high-resolution numerical model. *J. Geophys. Res.* 108, 3389. doi: 10.1029/2003JC001879

Zavala-Hidalgo, J., Romero-Centeno, R., Mateos-Jasso, A., Morey, S. L., and Martínez-López, B. (2014). The response of the Gulf of Mexico to wind and heat flux forcing: What has been learned in recent years? *Atmosfera* 27, 317–334. doi: 10.1016/S0187-6236(14)71119-1